Clinical Use of Electronic Portal Imaging :

Report of AAPM Radiation Therapy Committee Task Group 58

AAPM Refresher Course – Salt Lake City July 2001

Michael G. Herman
Division of Radiation Oncology, Mayo Clinic, Rochester, MN 55905

James M. Balter
Radiation Oncology Department, University of Michigan, Ann Arbor, MI 48109

David A. Jaffray
Radiation Oncology Department, William Beaumont Hospital, Royal Oak, MI 48073

Kiarin P. McGee
Department of Radiology, Mayo Clinic, Rochester, MN 55902

Peter Munro
Physics Department, London Regional Cancer Centre, London Ontario, CA N6A 4L6

Shlomo Shalev
Masthead Imaging, Nanaimo, BC CA V9R 2R2

Marcel Van Herk
Radiotherapy Department, Netherlands Cancer Institute, Amsterdam, The Netherlands

John W. Wong
Radiation Oncology Department, William Beaumont Hospital, Royal Oak, MI 48073

Table of Contents

TG58 is published in its entirety in Medical Physics Volume 28(5) pages 712-737. This presentation will review some critical information from TG58 and update the audience with current technologies and applications. This especially includes an update of references in each section of the manuscript.

I. INTRODUCTION

A critical requirement in radiation therapy is accurate day-to-day treatment setup. Early studies based on port films indicated the benefits of portal verification[1-4]. Numerous subsequent studies have characterized the magnitude and nature of setup errors for a variety of clinical conditions. Random and systematic errors of up to 6mm (σ) have been reported in previous studies[2,3,5-27].

An effective means to reduce setup error would be to increase the frequency of treatment verification with portal imaging[28]. Such action using port film is time consuming and labor intensive and can reduce throughput in a busy radiation therapy department. In addition, quantitative interpretation of geometric discrepancies is difficult and tedious to perform with non-digital imaging systems[29]. The need for an improved portal imaging system to enhance verification of conformal radiation therapy spurred the development of on-line electronic portal imaging devices (EPIDs).

The modern era of electronic portal imaging began in the early 1980s with demonstration by the late Norman Bailey of the use of a fluoroscopic system to acquire megavoltage transmission images[30]. The introduction of the scanning liquid ionization chamber system in 1990 was quickly followed by the introduction of camera-based fluoroscopic EPIDs from other manufacturers. At present, EPIDs are commercially available in the US from at least 5 vendors. Initially, these devices were embraced with great expectation by the radiation therapy community. At the time when Task Group 58 (TG58) was formed in 1995, about 250 systems had been sold in the US. In years since, informal surveys indicate that the initial promise has not led to wide spread clinical application of EPIDs. An informal survey of 69 institutions with EPIDs, conducted by members of TG58, indicated that 25% do not use the devices at all. The most common mode of operation is for the radiotherapists to perform visual inspection of the patient setup as a first-line of action to reduce large setup errors or mistakes. Only 50% of the surveyed institutions have secondary review stations and only half of these appear to have comprehensive analysis tools. About 40% of the institutions with EPIDs have developed a comprehensive quality assurance (QA) program, but fewer than half of these perform the program regularly. Thirty-five percent of respondents do not have a QA program at all. The majority of users surveyed consider image quality from current EPIDs inferior to that of port films and thus the EPID is not used, contrary to statements of superior EPID resolution repeatedly made in the literature. On the other hand, EPIDs are used because many users believe that these devices save time and provide quantitative feedback.

It is clear that EPID technology is under-utilized in the US. Furthermore, EPIDs are not used to produce their intended clinical benefit. Despite the impressive clinical results of European studies[31,32], it remains clear that apparent hurdles limit EPID utilization in the US. TG58 was formed to help AAPM members understand and implement EPID technology. It is the goal of this report to provide information to enhance and encourage effective use of these powerful devices.

The specific charges of Task Group 58 are:

1. To provide comprehensive technical information about the operation, limitations and system characteristics of the various commercially available EPIDs for the purpose of implementation, use and developing quality assurance programs.
2. To summarize existing experience on the effective implementation and use of the EPID for imaging in various clinical treatment sites and conditions from simple film replacement to quantitative statistical methods.
3. To describe tools currently available for on-line and off-line evaluations of the images.
4. To specify the requirements and discuss issues related to quality assurance for EPID systems, including the archive and management of the large amount of imaging data.

II. THE PHYSICS OF PORTAL IMAGING

Treatment verification usually involves comparison of a portal image acquired during a treatment fraction with a reference image that is generated prior to the initiation of the treatment course. Sometimes, the first approved portal image is also used as the reference image. While the portal image is formed by the megavoltage beam used to treat the patient, the reference image can be kilovoltage (e.g. simulation film), megavoltage or a digitally reconstructed radiograph (DRR).

It is generally accepted that the quality of images acquired using megavoltage x-rays is inherently poorer than that acquired with kilovoltage x-rays. Besides the well known decrease in subject contrast (e.g., the differential attenuation between bone or air and soft tissues) as the energy of an x-ray beam increases, many other factors contribute to the poor quality of portal images. These include the performance of the image receptor, x-ray scatter due to patient thickness, the size of the x-ray source, noise in the human eye-brain system, and (indirectly) the position of the image receptor. The purpose of this section is to explain how these factors influence the portal image quality and to understand the fundamental limitations of imaging with megavoltage x-ray beams. This in turn should help readers understand what they can and cannot expect from the imaging performance of EPIDs.

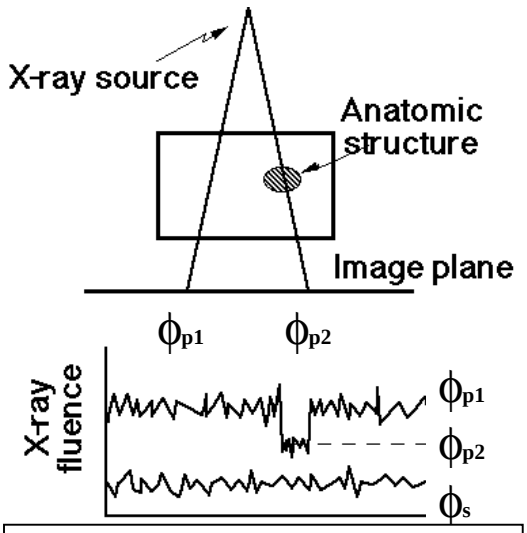

Fig.1 Schematic representation of the imaging process. Fluences ϕ defined in text.

A number of key quantities give an objective measure of image quality. Figure 1 illustrates the image formation process and its relation to some key indicators of image quality. This chapter addresses contrast, noise, spatial resolution, detective quantum efficiency (DQE) of EPIDs and X-ray scatter.

A. Contrast

Contrast, C, describes how much an object stands out from its surroundings and is defined as[33]

$$C = \frac{signal}{mean\ signal} = \frac{\phi_{p2} - \phi_{p1}}{(\phi_{p2} + \phi_{p1} + 2\,\phi_s)/2} \qquad (1)$$

where ϕ_{p_1}, ϕ_{p_2}, and ϕ_s are the primary and scatter photon fluences reaching the image receptor (Fig. 1). Motz and Danos have shown that this expression can be re-written as[33]

$$C = \frac{2(1 - e^{-\Delta})}{1 + e^{-\Delta} + \frac{2\,SF}{1 - SF}} \qquad (2)$$

where: Δ is the difference in attenuation between the object and the background (i.e. $\Delta = L_x|\mu_{bone} - \mu_{water}|$), μ_{bone} and μ_{water} are the x-ray attenuation coefficients for bone and water, respectively, L_x is the thickness of the anatomic structure, and SF is the scatter fraction {$SF = \phi_s/(\phi_s + \phi_p)$}. Equation 1 shows that the contrast is increased by increasing the difference in attenuation along the x-ray path and is decreased by the addition of a scatter fluence.

Subject contrast of 1 cm thick bone or air objects embedded within 20 cm of water as a function of x-ray energy can be calculated using Equation 2. For simplicity, the contrast has been calculated assuming that no x-ray scatter occurs (i.e., SF = 0). For comparison purposes, 50 kev approximates the mean energy of the x-ray energy spectra used to generate a simulator image (100 kVp, diagnostic energy) and 2 MeV that of the 6 MV beam to generate a portal image. Examining the subject contrast at these two x-ray energies shows the subject contrast decreases from 0.5 to 0.037 (a factor of 13) for the bone and from 0.2 to 0.05 for the air pocket (only a factor of 4). This explains the enhanced visibility of the air passages relative to bony anatomy seen in the therapy image as compared to the simulator image.

Contrast is the result of differences in x-ray attenuation within the patient. At low energies, the photoelectric process dominates. Since the photoelectric cross-section is proportional to the atomic number raised to the third power (Z^3), the higher atomic number of bone results in a larger attenuation coefficient compared to that of water. However, the photoelectric cross-section is also inversely proportional to the energy cubed ($1/E^3$). Compton scattering becomes the dominant interaction process above 20 keV for soft tissues and above 50 keV for bone (assuming that the atomic number of bone is ~13). The Compton scattering cross-section is dependent on the electron density of a material, which, except for hydrogen, varies only slightly with atomic number. The electron density of water (ρ_e(water) = 3.34×10^{23} electrons/cm^3) is comparable to that of bone (ρ_e(bone) = 5.81×10^{23} electrons/cm^3). Therefore, the difference in attenuation, and hence the contrast, reduces significantly at megavoltage energies.

B. Signal to Noise Ratio

Quantum Noise

The most important concept to understand is that image quality (or "detectability" of bony anatomy) is ultimately determined <u>not</u> by the subject contrast of the object being imaged but by the signal-to-noise ratio (SNR) of the image. A number of sources of noise contribute to the

SNR. A limiting source of noise is due to x-ray quantum statistics. This is best explained again with Figure 1, which shows the process of x-ray image formation. The difference in attenuation between an object and its surroundings (i.e., subject contrast) results in different number of x-ray quanta reaching and interacting in an image receptor. The subject contrast is determined by the energy of the x-ray beam, the radiological properties of the object being imaged, and the amount of x-ray scatter reaching the image receptor. However, since image formation is a statistical process involving the detection of discrete x-ray quanta, there will be a statistical uncertainty (known as x-ray quantum mottle) in the number of x-ray quanta that interact in the image receptor. The detectability of the object therefore depends not only on how large the difference in attenuation is between the object and its surroundings, but also on how large this signal difference is compared to the uncertainty in the signal, i.e. SNR.

The number of x-ray quanta detected in some time interval follows Poisson counting statistics. For a Poisson process, the variance in the number of detected x-ray quanta is equal to the mean number of detected photons. Therefore, if the mean fluences are known, a signal-to-noise ratio can be calculated. The signal-to-noise ratio of the bone signal shown in Figure 1 is calculated as

$$SNR = \frac{image\ signal}{noise} = \frac{\phi_{p2} - \phi_{p1}}{\sqrt{(\phi_{p2} + \phi_{p1} + 2\,\phi_s)/2}} \qquad (3)$$

Rewriting in terms of the geometry shown in Figure 1, we obtain

$$SNR = \sqrt{A \cdot \phi_i \cdot T \cdot \eta}\ \frac{2(1 - e^{-\Delta})}{\sqrt{1 + e^{-\Delta} + \frac{2\,SF}{1 - SF}}} \qquad (4)$$

where: A is the area of the detector element, ϕ_i is the incident fluence, T is the patient transmission, and η is the x-ray detector efficiency. Equation 4 shows that the SNR, like the contrast, decreases as the difference in attenuation between the object and the background (Δ) decreases. However, unlike the contrast, the SNR is proportional to the number of x-rays detected ($A\cdot \phi_i \cdot T \cdot \eta$ = the area x fluence x transmission x collection efficiency = number of detected x-rays). In addition, scatter reduces the SNR by adding noise without contributing to the signal.

The SNR versus x-ray energy for an image of a 1 cm thick bone in 20cm of tissue can be calculated using Equation 4. A typical diagnostic imaging procedure delivers a dose of 0.05 cGy (50 mR) to the patient[34]. For the same patient dose at megavoltage energies, the SNR would be ~100 times smaller. While the diagnostic SNR would satisfy Rose's criteria for visibility (SNR=5)[33], the megavoltage beam would not (Table I). However for the same photon fluence, a megavoltage beam delivers more dose. Doses more common in megavoltage imaging are also shown in Table I.

Table I. Calculated SNR and patient doses at diagnostic and therapeutic x-ray energies.

Energy	Diagnostic (50 keV)	Therapeutic (2 MeV)	Therapeutic (2 MeV)	Therapeutic (2 MeV)	Therapeutic (2 MeV)

Patient Dose	0.05 cGy	0.05 cGy	1 cGy	10 cGy	55 cGy
SNR	71	<1	4.8	15	35

This simple model demonstrates that subject contrast decreases with increasing x-ray energy. Not only does the contrast of objects decrease, the rate of decrease depends on the effective atomic number of the object. This results in the contrast of air passages exceeding that of bony anatomy when x-ray energy exceeds 100 keV. Furthermore, the SNR of the bone signal decreases rapidly with increasing energy. For the same dose to the patient, the SNR is much lower at megavoltage energies (2 MeV) than that at diagnostic energies (50 keV). For typical diagnostic and therapy doses of 0.05 cGy and 10 cGy respectively, the gap in SNRs is reduced. The SNR is only 5 times lower at megavoltage energies.

Quantum Efficiency

While quantum noise affects image quality, the efficiency of propagating the quanta through to the final detection stage can have a large impact on the SNR. An analysis of the detective quantum efficiency (DQE) of an imaging system determines the magnitude of this effect. While a thorough introduction in DQE is beyond the scope of this report (see e.g. reference [35]), a brief example of the impact of DQE on the design of one component of the imaging chain is presented. The DQE is a measure of how efficient the imaging system is at transferring the information contained in the radiation beam incident upon the detector. This is expressed as the square of the ratio of SNR output to SNR input as a function of spatial frequency.

The image receptor should always have high quantum efficiency so that a large fraction of the incident x-ray quanta actually will interact in the receptor. In reality, portal imaging generally operates with low quantum efficiency. All commercial portal imaging systems use a metal plate (x-ray converter) to convert photons to Compton electrons. In video-based EPIDs, a phosphor screen is used to convert the electrons into optical photons. A scanning liquid ion chamber directly detects ionization due to the electrons. While ~4% of the incident x-ray quanta interact in the metal plate, less than 1% of the incident x-ray quanta will generate electrons that exit from the metal plate, propagating quanta further down the imaging chain. Figure 2 shows the quantum efficiency of a 1 mm copper plate in contact with different thicknesses of phosphor screens, when irradiated by a 2

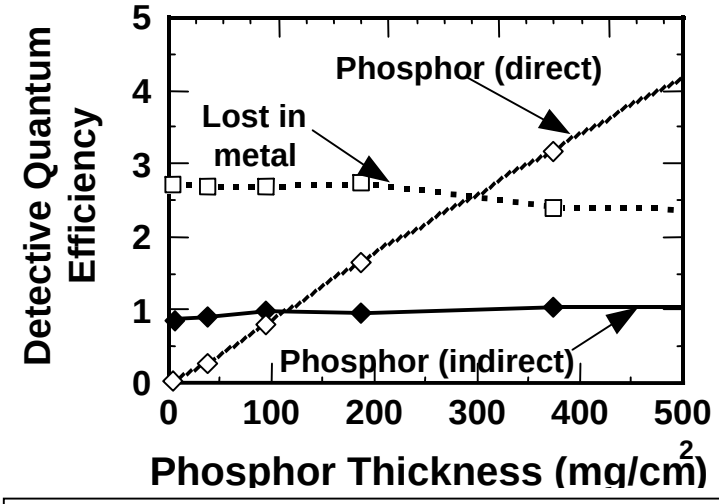

Fig 2. DQE for different phosphor screens. The "phosphor (indirect)" curve represents those quanta that first interact in the copper plate and deposit energy in the phosphor screen. The "lost in metal" curve represents those quanta that interact in the metal plate but do not deposit energy in the phosphor screen.

MeV x-ray beam (calculated using the EGS4 Monte Carlo code). Conventional portal film, exposed under a metal plate, with no phosphor, has a quantum efficiency of ~1%.

Figure 2 shows that the quantum efficiency increases as the thickness of the phosphor screen increases, because the incident x-ray quanta can also interact directly within the phosphor screen[36]. Therefore, somewhat fortuitously, the need for a phosphor screen increases the quantum efficiency of commercial EPIDs. For example, a phosphor screen thickness of 200 mg/cm^2 (in a camera-based EPID) has a quantum efficiency ~2.5 times greater than the conventional cassettes used for portal films. A similar argument can be made for the liquid in the scanning ion chamber systems, with a thickness of ~80 mg/cm^2, yielding a quantum efficiency of 1.5 relative to film.

Direct approaches to increase quantum efficiency by increasing the thickness and/or density of the metal plate x-ray detectors are often ineffective. Typically, spatial resolution deteriorates due to the increased extent of the x-ray deposition region. For the commercial camera-based EPIDs, thick phosphor screens are often employed. In addition to the loss of spatial resolution and optical light transmission, thick screens are prone to non-uniformity in phosphor content, and thus add to the structure noise of the imaging system. It is unlikely that increasing the thickness of the phosphor screens will yield further benefits.

Other Sources of Noise

The above analysis of SNR and quantum efficiency is based on *primary x-ray quantum noise only* and does not include other sources of noise, each of which can have a major effect on the image quality. There are a large number of other noise sources in any portal imaging system, including energy absorption noise[37], noise added by the imaging system and noise in the human visual system.

Note that the small amount of information from the x-ray beam extracted by all EPIDs and portal films still represents a very large amount of detected x-ray quanta. Indeed, at typical exposure (or dose) used for imaging, the x-ray fluence reaching the image receptor is generally 100 times greater at megavoltage energies than at kilovoltage energies[38]. It appears poor image quality is not because the image receptors do not have enough x-ray quanta interacting in them, but because the image receptors either add additional noise to the images or display the images so that noise in the eye-brain system becomes important.

Measurements of Munro et.al.[39-41] suggest that conventional portal films record more information than EPIDs, but the experience of EPID users and contrast-detail studies[42] suggest that improved display of portal images by EPIDs reduces the effect of observer noise[43] inherent in visual film observation. This is due to the superior contrast resolution of the EPID and the ability to process the images and more than compensates for the smaller information content.

The ideal image receptor would be an EPID or film that adds no electronic or film noise to the image and which displays the image optimally. Recent developments, such as EC-L film and amorphous silicon EPIDs, come close to meeting this ideal.

C. Spatial Resolution

Another important factor that influences image quality, but which is not included in the model described above, is spatial resolution. Spatial resolution is a measure of how the image signal is blurred by the imaging system. For example, the spatial resolution of the system influences how well edges, such as those resulting from bones, will be detected. The spatial resolution of commercial EPIDs depends on factors that are common to all EPIDs as well as

factors that are device specific. The spread of high energy particles in the metal plate is common to all commercial EPIDs and is quite modest[44,45]. In addition to the lateral migration of high energy electrons, other processes such as x-ray scatter, bremsstrahlung, and positron annihilation, also contribute to the signal spread in the metal plate[36,39,45]. Once the high energy particles exit from the metal plate they can spread in the convertor (phosphor screen, ionizing fluid). While lateral electron migration would be greater in the ionizing fluid (~ 0.8 g/cm^3) than in the phosphor screen (~ 3.74 g/cm^3), it is light spread in the phosphor screen[39] that mostly determines the spatial resolution for the camera-based EPIDs. Pixel size is the primary factor that determines the spatial resolution for the matrix ion chamber EPID[46].

The spatial resolution of an imaging system is often characterized by examining how well the system reproduces a point object (infinitesimally small). Acquiring an image of such a point object measures the system's point spread function. Conventionally, this spread of signal is represented in the form of the modulation transfer function (MTF). The MTF describes how well the system passes different spatial frequencies and is calculated from the Fourier transform of the point spread function. Any complete characterization of an imaging system requires an examination of both the signal-to-noise characteristics and the spatial frequency response of the system.

It is a common misconception that the spatial resolution of the imaging system is the major factor limiting the image quality of portal films and portal images. Spatial resolution of any portal image depends upon three quantities, the size of the x-ray source, the spatial resolution of the image receptor, and image magnification. Source sizes of medical linear accelerators have been measured to be ~ 1 mm full width at half-maximum, or smaller. Other measurements have shown that the line-spread functions for camera-based EPIDs are 0.8-1.0 mm[39,47] full width at half maximum while that for the matrix ion chamber EPID is 1.5-2.0 mm.[46] Image magnification is variable and can have an important effect on the spatial resolution of the system. As the magnification increases, geometric blurring due to the x-ray source increases, while the size of the patient anatomy projected at the plane of the image receptor also increases, reducing the effect of blurring by the image receptor. Thus, there is an optimal image magnification where the blurring due to both the image receptor and the x-ray source is minimized. Calculations suggest that the optimal image magnification is between 1.3-2.0, which fortunately encompasses the range of operation for almost all commercial EPIDs.[48,49]

Finally, in portal imaging, it is important to recognize that there is reduced attenuation at megavoltage energy (compared with kilovoltage), which results in the reduced sharpness of the object and an apparent change in the projected object dimension. This leads to the perception that portal images have lower spatial resolution than diagnostic images. Care must be taken when comparing images acquired with different photon energies.

D. X-ray Scatter

Scattered x-rays, or any “non-primary” photons, can reduce the subject contrast and the signal-to-noise ratio of portal images (see Figure 1) by generating signals in the image receptor that carry no geometric information about the patient’s anatomy but that add noise to the images. The reduction of contrast by x-ray scatter is of serious concern for portal films, since the display contrast of film cannot be adjusted to compensate for any reduction in subject contrast. For EPIDs, the reduction in signal-to-noise ratio due to x-ray scatter is more important than the reduction in contrast. While x-ray scatter has long been a major concern in kilovoltage x-ray

imaging, it has been shown that it is much less of a problem for megavoltage portal imaging.[48,50] As the energy of the x-ray beam increases, the scatter fraction (the fraction of the total fluence reaching the image receptor that is due to scattered x rays) decreases from 0.9 at 100 keV to less than 0.6 at 6 MV (at the exit surface of the patient). (On the other hand, scattered component of kilovoltage beams can be reduced substantially using grids, which is not possible for megavoltage beams.) As in diagnostic radiology, geometric factors are quite important in influencing the scatter fluence reaching the image receptor at megavoltage energies. The scatter fraction increases as the patient thickness increases, as the field size increases, and as the air gap between the patient and the image receptor decrease. Apart from extreme situations such as very large patient thicknesses and field sizes, and small air gaps, x-ray scatter generally does not degrade the image quality of portal image significantly. Jaffray et.al. have shown, using Monte Carlo calculations, that the signal-to-noise ratio would improve by less than 10% if all x-ray scatter were eliminated before reaching the image receptor when a moderately thick (20 cm) patient is irradiated.[50]

III. THE TECHNOLOGY OF MEGAVOLTAGE IMAGING

Many different EPIDs have been examined since the early 1980's as alternatives to film for megavoltage imaging. The readers are referred to four comprehensive reviews of portal imaging devices for further details.[51-54] Commercially available systems consist of matrix ion chamber EPIDs, camera-based EPIDs, and the newest systems based on active matrix flat panel imaging (AMFPI) technology.

A. Matrix Ion Chamber

The matrix ion chamber device (originally developed by Meertens, van Herk and their colleagues) consists of two sets of electrodes that are oriented perpendicularly to each other separated by a 0.8-mm gap, which is filled with a fluid (2,2,4-trimethylpentane) that is ionized when the device is irradiated.[55] Each set of electrodes consists of 256 wires spaced 1.27 mm apart to provide an active area of 32.5 cm on a side. One set of electrodes is connected to 256 electrometers and the other set of electrodes is connected to a high-voltage supply that can apply a 300-V potential to each electrode individually. The matrix ion chamber array is read out by applying a high voltage to each of the high-voltage electrodes in succession (for approximately 20 milliseconds) and measuring the signal generated in each of the 256 signal electrodes. This procedure takes 5.5 seconds to read out an image. In addition, a fast (lower resolution) scanning mode is available that scans the array in 1.5 seconds by applying the high voltage for a 10 millisecond period to two high voltage electrodes at a time. The fast acquisition mode is useful for acquiring double-exposure images. The more recent systems operates with a high voltage bias of 500 volts and at rate of 5-millisecond readout per electrode giving an entire image read out time of 1.25 seconds.

The most obvious advantage of the matrix ion chamber is its compact size, which makes the device a convenient replacement for film cassettes. Another advantage is its geometric reliability--images acquired with the system have no geometric distortions. The major limitation of a scanning radiation detector is quantum utilization, since only one high-voltage electrode (out of 256) is active at any one time. However, the physics of signal generation in the 2,2,4 trimethylpentane improves the quantum utilization of the matrix ion chamber considerably. The signal measured by the matrix ion chamber depends on the rate of formation and the rate of recombination of the ion pairs that are generated in the ionizing fluid. Even when no high

voltage is applied to the electrodes, the rate of recombination of the ion pairs generated in the 2,2,4 trimethylpentane is relatively slow. Therefore, the concentration of ion pairs can increase over a period of time until an equilibrium is reached between ion-pair formation, and is a function of the dose rate at the matrix ion chamber and ion-pair recombination, the latter is proportional to the square of the ion-pair concentration. The rate of ion-pair formation as a function of irradiation time in the absence of high voltage bias is shown in Figure 3.

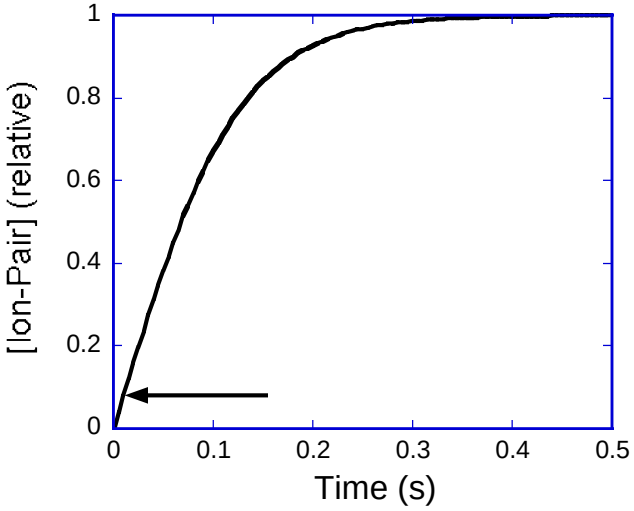

Fig 3 The relative ion-pair concentration in the matrix ion chamber as a function of irradiation time. The equilibrium concentration depends on dose rate. The horizontal arrow represents the signal that would be measured in a 10 ms period if no charge integration occurred in the ionizing fluid

In effect, the signal measured by any electrode of the matrix ion chamber does not depend greatly on the dose rate during the 5-20-millisecond period when the high voltage is applied but on the previous irradiation history of the electrode. However, the effective period of the charge integration (0.5 second) is still short compared with the total image acquisition time. Therefore, a large fraction of the radiation that interacts with the matrix ion chamber does not generate any measurable signal. For this reason, the matrix ion chamber requires higher doses to generate images than other portal imaging devices. Note that once the latent image has been formed, the more rapidly that the image can be read out, the smaller the dose to the patient is required to form an image.

Fig 4 AP pelvis with SLIC EPID

An example of an AP pelvis field acquired with the matrix ion chamber EPID is shown in Figure 4. Since spurious (dark) signals can be generated in the electrometers and ion chambers, and because the sensitivities of each ion chamber can vary, the raw signals from the matrix ion chamber EPID must be processed before yielding a usable image. For similar reasons, calibration of the system on a monthly basis ensures its optimal operation. Because the matrix ion chamber is a scanning EPID, it is susceptible to artifacts if the dose rate of the accelerator changes during image

acquisition. Thus, the radiation beam has to stabilize for some period (typically 1.0 s) after start-up before image acquisition can begin. The best image quality results when the scanning of the high voltage electrodes is synchronized with the pulsing of the linear accelerator. In practice, the matrix ion chamber EPID needs to be calibrated for each of the dose rates of the accelerator that will be used clinically. Finally, many of the radiation sensitive readout electronics are located immediately adjacent to the active region of the matrix ion chamber. Even with the use of electronic components that have improved resistance to radiation damage, care must be used to ensure that the field size or the position of the EPID is coordinated to prevent accidental irradiation of the electronics.[56]

Van Herk et al. have characterized the MTF and DQE of the system by correcting for the non-linear response of the system. Figures 5a and 5b show the fitted pre-sample line spread function (LSF) and the corresponding MTF of the latest matrix ion chamber EPID. Horizontal and vertical directions are with respect to the image detector. The detector has a high sensitivity all the way up to the Nyquist frequency. Two effects may cause the significant difference between the horizontal and vertical resolution. First, the 256-electrometer amplifiers include a filter with a time constant of about 1 ms, which may cause some blurring in the vertical direction. Second, the absence of shielding between the ionization chambers may cause some spurious sensitivity outside the pixel area due to the direction of the electric field lines.

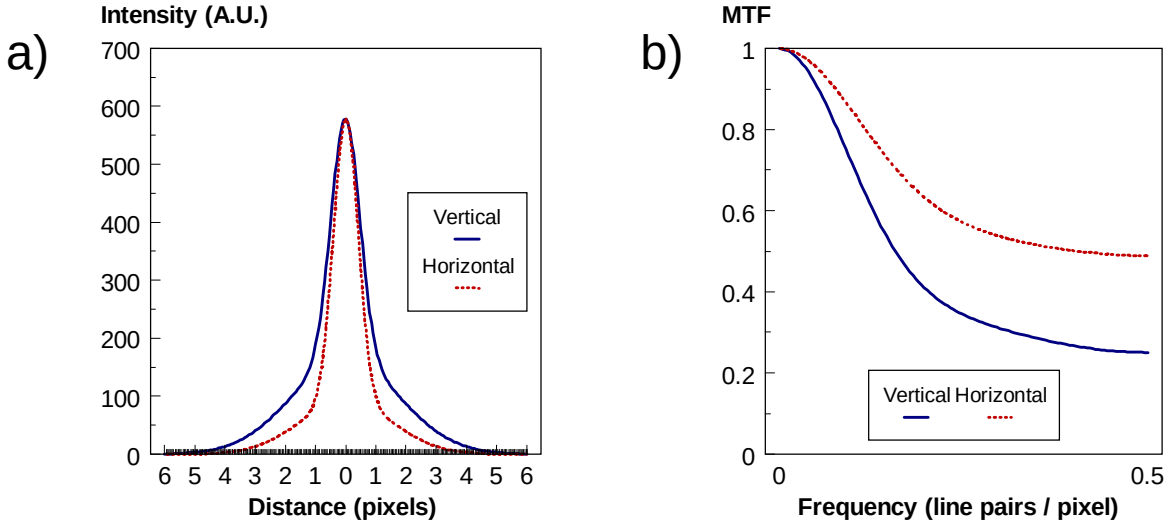

Fig 5 - a) Fitted pre-sampling line spread functions (LSF), normalized on the central value. b) Modulation transfer functions (MTF).

The zero-frequency DQE depends strongly on the dose per image (Figure 6). In contrast to linear detectors, where the DQE decreases with decreasing dose (due to the influence of system noise), the DQE increases for this detector. This effect is caused by the increase in integration time at lower dose rates due to the latent image in the liquid. The ratio between the DQE and the sampling efficiency gives the inherent efficiency of the metal plate detector, which would be reached at 100% sampling efficiency. Decreasing the readout time (which improves the sampling efficiency) may therefore further improve the DQE. Efforts are being made to further characterize the frequency dependence of the DQE for the matrix ion chamber EPID.

In addition to the detection electronics, a typical liquid ion chamber EPID has a gantry mounted robotic arm that provides complete retraction of the unit.

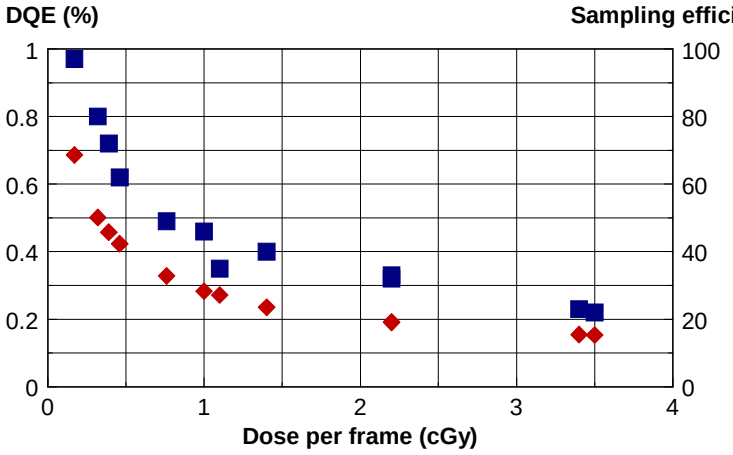

Fig 6 - Detective Quantum Efficiency (DQE) and sampling efficiency of the matrix ionization chamber device

B. Camera-Based EPIDs

Camera-based systems consist of a metal plate and a phosphor (gadolinium oxysulfide (Gd_2O_2S)) screen viewed by a camera using a 45° mirror. When irradiated, high-energy electrons generated in the metal plate and the phosphor screen are converted into light in the phosphor screen and this light creates the video signal generated by the camera. The video signal from the camera can be digitized and the digitized image can be viewed on a monitor located in the control area of the accelerator. The video systems differ primarily in the deployment of their housing assembly (see Table II – See Table VII for aSi Specifications) and camera operation. Various techniques for readout are designed to reduce the impact of noise in the imaging chain.

Video EPIDs suffer from the major limitation of light collection efficiency of the optical chain. Since the light is highly scattered within the phosphor screen, the light is emitted from the rear of the screen in all directions with equal probability. Only those light photons that are emitted within a small cone subtended by the lens of the camera can generate a signal in the camera; typically only 0.1-0.01% of the light emitted by the phosphor screen reaches the camera. This poor light collection efficiency reduces image quality in two ways. Firstly, if an x-ray photon interacts in the x-ray detector but none of the light generated by this interaction reaches the camera, then no measurable signal is produced. Secondly, if only a small signal is produced in the camera, then noise generated by the pre-amplifier and other electronics of the camera may be large compared to the signal. As a result, the development of commercial camera-based EPIDs has focused on increasing light collection of the optical chain by increasing the thickness of the phosphor screen to increase the light output and to a smaller extent increase the x-ray quantum efficiency,[42,47] and using a large aperture lens that collects more of the light.[42,52]

The use of large aperture lenses suffers from decreased spatial resolution because of spherical aberrations (light rays reaching the edges of the lens do not focus to the same point as those reaching the center). The spatial resolution of these lenses decreases from the center to the edge of the lens. There is also a reduced depth of field which renders the focal distance more sensitive to optical wavelength. Large aperture lenses also suffer from vignetting, which results in images that are brighter at the center of the lens than the edge. This change in image brightness is corrected through software or hardware schemes. Finally, large aperture lenses can generate distortions, such as pin cushion or barrel distortion, which cause straight lines to appear curved in

the image, especially at the edges of the field of view. Examples of the MTF and zero frequency DQE of a camera-based EPID from camera-based system are shown in Figure 7.

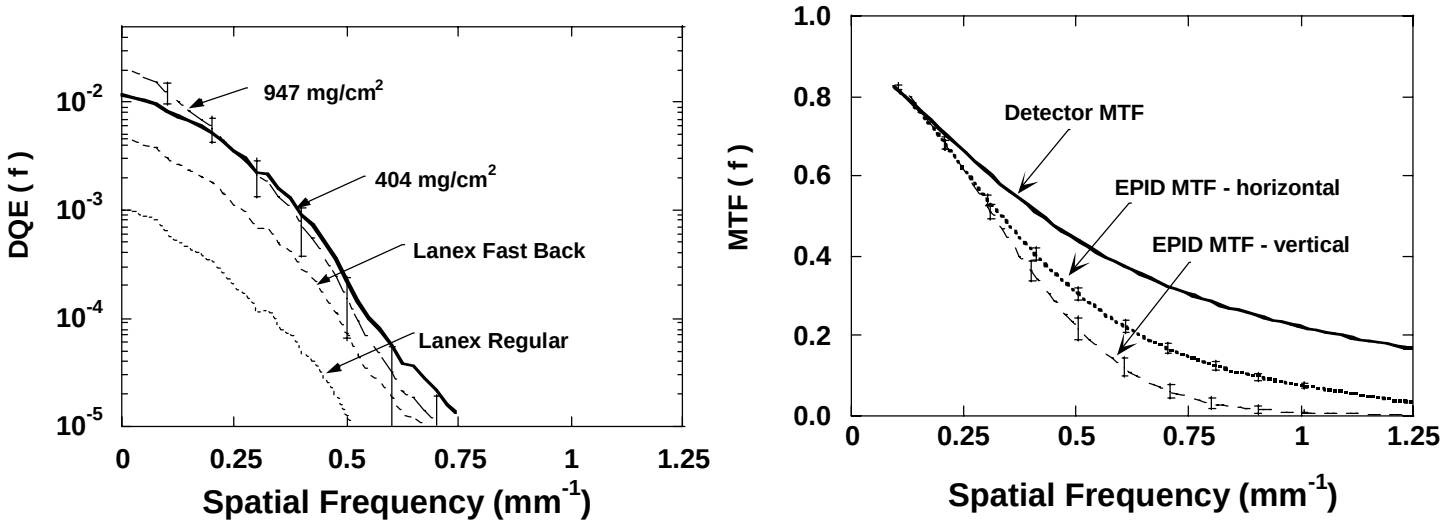

Fig 7 - a) MTF, Video EPID, b)DQE, Video EPID.

An image acquired with 2-monitor units at 6 MV with this system is shown in Figure 8. Image 8a was corrected for lens vignetting, while image 8b shows improvement from simple image enhancement tools such as level and window and contrast adjustment.

There are a variety of mounting systems for video based EPIDs that range from rigid gantry mounts, partially or completely retractable systems to systems independent of the gantry on a portable stand.

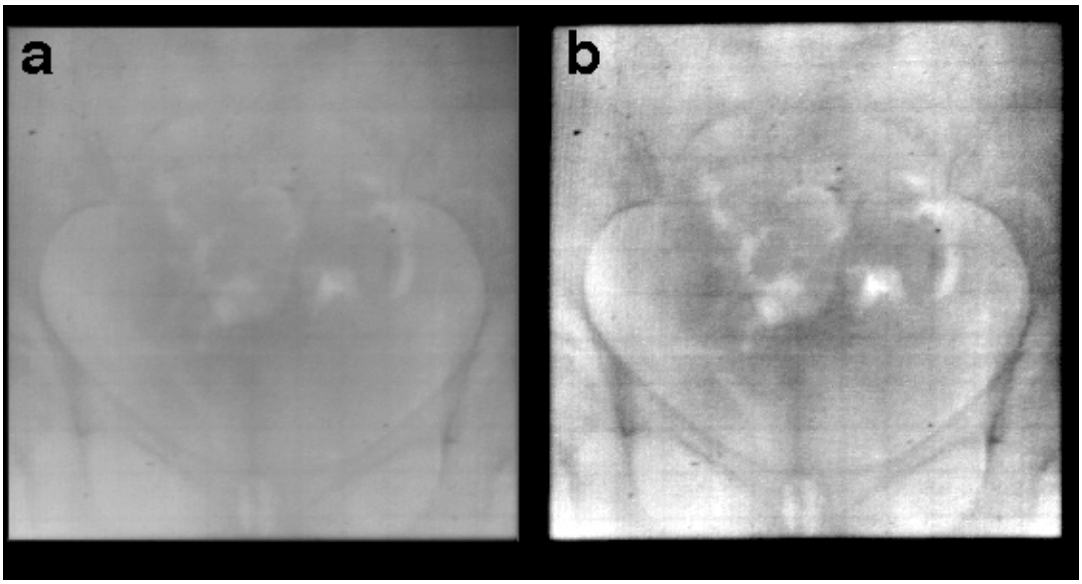

Figure 8 - Video EPID Image a) and b) with enhancement

C. Flat Panel Detectors

Flat panel or AMFPI detectors are currently divided into two types, Silicon or photodiode systems and Selenium or photoconductor systems. Initial development work with flat panel detector systems has been detailed in the literature. In either case, the image quality from the flat panel devices is superior to that of the liquid ion chamber or the video EPIDs.

Amorphous Silicon

References for this type of detector. [50,57-74]

The amorphous silicon EPID consists of a copper plate, a gadolinium phosphor screen and a flat-panel light sensor coupled to readout electronics (Figure 9). These devices have pixel pitches of less than 1mm. Each pixel in the flat-panel light sensor consists of a photodiode, which detects the light emitted by the phosphor screen, and a thin film transistor (TFT), which acts like a switch to control the readout of the signal. During irradiation, light that is generated in the phosphor screen discharges the photodiode, which has a 5 V bias voltage applied before the irradiation. The TFT is non-conducting during this period. During readout, the TFT is made conducting and this allows

Fig. 9 -

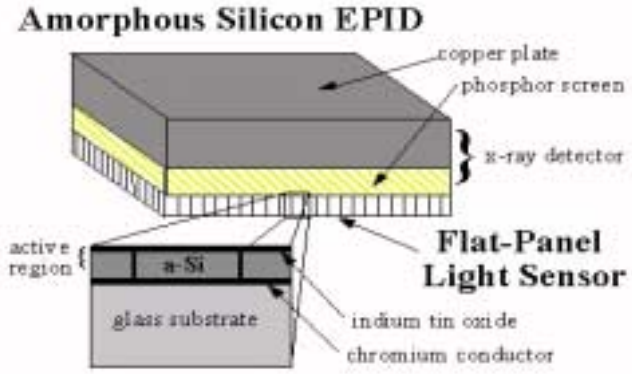

current to flow between the photodiode and an external amplifier. The photodiode is recharged to its original bias voltage and the external amplifier records the charge. This charge is proportional to the light reaching the photodiode during the irradiation. By activating the TFT's one line at a time and by having all of the TFT's in one column connected to a common external amplifier, the signals generated in the flat-panel light sensor can be read out one line at a time with a modest number of electronic components. Readout frame rates of up to 30/s are achievable. The DQE is shown for various aSi measurements, compared to a video EPID in Figure 10 from Peter Munro.

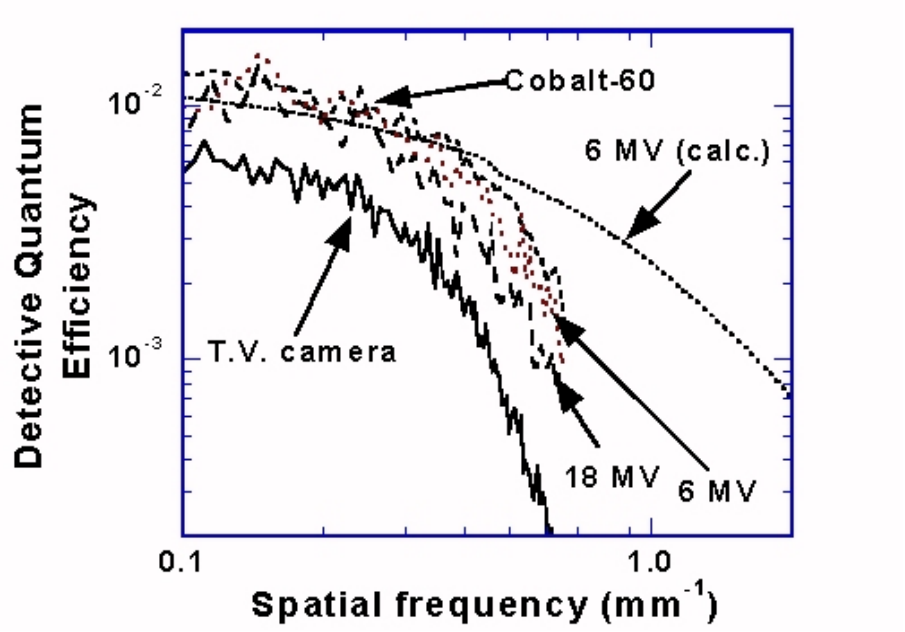

Fig. 10 – DQE for an aSi EPID, measured and calculated compared to a video EPID.

Figure 11 shows an example image indicating the excellent image quality of the aSi imagers at megavoltage energies.

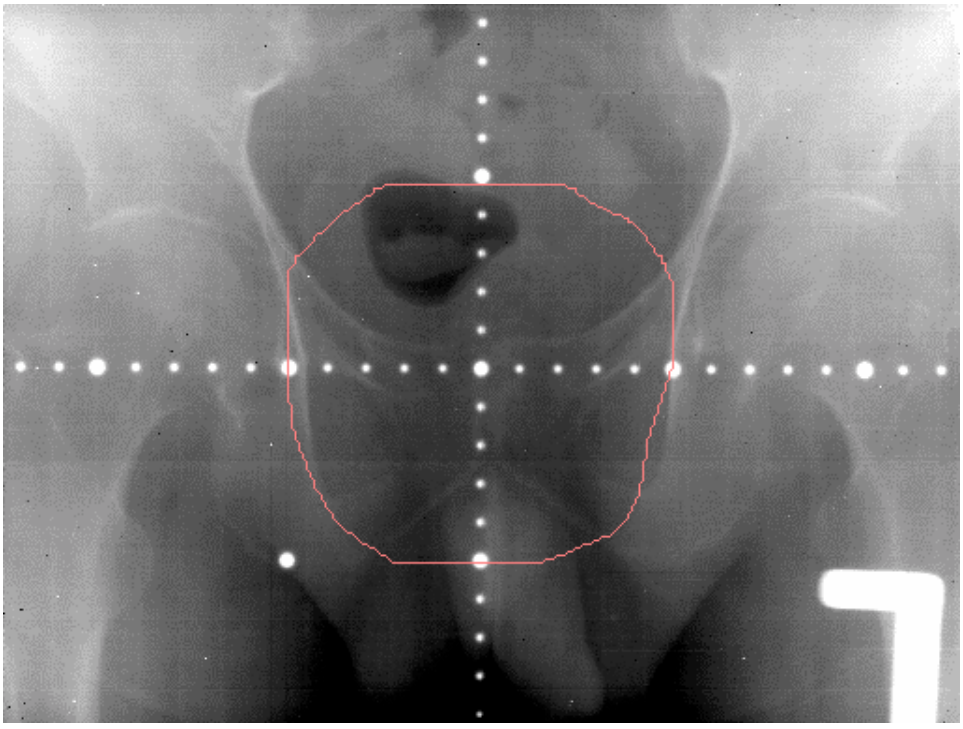

Fig. 11
AP aSi image from Varian Portal Vision

Amorphous Selenium

Similarly the selenium systems are composed of a flat panel detector. The primary difference is that the detector array is a photoconductor of a-Se, deposited on a metalic substrate, which forms a direct x-ray detector, with no need for a metal converter plate and phosphor screen (refer to figure 9). The systems can be read out either by electrostatic methods, or actively with TFT as in the a-Si systems. [75-85]

A sample image from an aSe detector is shown in figure 12.

Fig 12 – aSe megavoltage image: Dr. G. Pang, Toronto Sunnybrook Regional Cancer Center

IV. Commissioning and Quality Assurance for EPIDs

A. Installation and Commissioning

At the time of installation/acceptance the following features must be verified: mechanical and electrical safety, geometric reproducibility, image quality and software performance specifications. Following acceptance, commissioning will characterize operational features relevant to clinical use and specifications for routine quality assurance. The items discussed in detail here are summarized in Table III.

Some elementary safety aspects of EPID should always be checked, even if the devices are not used regularly. While one should adhere to the manufacturer's maintenance manual, if available, the following list contains a few of the basic tests that should be considered.

a) Mechanical stability and integrity of EPID mounting and casing. The most serious risk is dropping the device on a patient or therapist during gantry rotation. Particular attention should be placed on checking the mounting point for detachable EPIDs and gears for retractable or movable EPIDs.

b) Operation of collision detection system. The most serious potential hazard is the EPID colliding with the patient.
c) Electrical insulation/grounding. The most serious potential hazard is potential electrocution of patient or staff. Most systems are grounded through the power outlet connected to the control computer and/or interface unit. The power supply insulation must be checked. One should also examine the cabling to the detector. The Varian PortalVision Mark 1 carries 300 volts to a plug-on detector cassette (but the improved Mark 2 generates the applied 500 volt internally from the +15 volt on the cable). Any moving cable or cables that potentially reach the patient or staff should be inspected visually once a month.

The Varian PortalVision detector contains a volatile liquid. In case of a collision, the device should be powered off and should be checked for any damage to the detector array. However, such damage is relatively unlikely since the actual array is under 2 cm of Styrofoam. Leakage of the liquid can be identified by a large change of the sensitivity of the central part of the detector. In such a case, the detector should be removed from service.

Dose Control

Optimizing the dose necessary for imaging is important and varies by application and EPID. Improper dose control could cause failure to complete acquisition of a useful verification image in the pre-set dose (resulting in a useless image and extra dose required for obtaining a subsequent image), and over-dosage due to a failed beam-off signal. Most EPIDs have adjustable trigger levels or delay times to allow the accelerator output to become stable.[5,6] The dose delivered for a localization image can be pre-set in three ways: by manual beam interruption (not preferred, since operator errors might lead to a large dose), by a pre-set dose or by auto-beam off. One should test correct image acquisition with different attenuators or an anthropomorphic phantom in the beam. Reducing the dose required for localization images is possible in video systems by using short exposure times (with some reduction in image quality), but the PortalVision has a predetermined acquisition time. For the latter, the use of a low dose rate is desirable. A complete test of the EPID-linear accelerator control system including the information system, which may contain parameters that are downloaded to the EPID or linac, must be performed prior to clinical use.

Calibration

Most EPID systems require some form of image calibration. Calibration provides correction factors and measures accelerator and EPID characteristics that are used to produce the highest quality image in routine use. Often, background signals are subtracted and inhomogeneity of response as well as linear accelerator beam characteristics are divided out. One should be aware that noise in the calibration images can reduce clinical image quality and should be minimized. The EPID must be calibrated for the varying conditions of clinical image acquisition. Calibration procedures depend on the type of EPID and vendor recommendations, however in each case it involves exposing the EPID to radiation under specific conditions. Calibration usually includes measurement of a dark current or noise image. This is acquired with no beam and represents signal present in the EPID when there is no radiation beam. This is followed by the acquisition of a full open field. The open field image is used to correct for reproducible treatment field specific characteristics, such as variation of intensity across a beam profile. Since beam characteristics may be beam energy and field size dependent, calibrations at various energies and field sizes must also be made. The information is used to generate correction factors used in the image acquisition process. In some cases, scatter and attenuation introduced by the

patient can affect image quality and patient thickness and detector distance are therefore considered calibration parameters. The EPID may even require gantry angle calibration, if the mechanical stability of the EPID is such that a mechanical shift offsets the calibration of a flat field, or the treatment machine characteristics change significantly at varied gantry angles. The user is encouraged to determine which characteristics are most important for the EPID chosen, to insure optimal operation.

Test image acquisition should be performed using the fresh calibration to ensure absence of artifacts due to accelerator instability or objects in the beam. While table grids and patient supporting plates appear as distractors in images, they are never sufficiently stable to be removed by calibration. The frequency of re-calibration depends on the measured stability of image performance. Typically, a monthly re-calibration may be necessary depending on the mechanical stability of the device. If any of the optical components in a fluoroscopic system are altered, a re-calibration is recommended.

Linearity

The linearity of imaging geometry should be established during commissioning. Spatial distortions must be characterized or removed from EPID images before they can be used for quantitative portal imaging. Lack of rigidity in EPID components of video systems may result in instability of magnification or spatial linearity. EPID systems that use an analog video camera are susceptible to distortions due to variations in magnetic field and may depend on gantry angle. Bending or displacement of mirrors or front screens may also cause distortions. Simple mechanical phantoms (square grid of pins) to test for distortions are available from the manufacturer or easily fabricated.[86,87] The use of fiducial markers or field edges to quantify patient setup errors can eliminate mechanical instability effects.

The reproducibility is established by checking both position (location and orientation of projected collimator axes) and linearity as the imager is repeatedly repositioned. This should also be performed at various gantry angles.

Image Quality

Clinical image quality commissioning is based on spatial resolution and contrast resolution. All present day EPIDs provide 1% or better contrast resolution for larger objects (>5mm). These characteristics are sufficient to perform portal localization on most radiotherapy fields. The Las Vegas phantom (Figure 13) has been used in acceptance testing and continuing QA. It is composed of varying thickness and varying width holes embedded in aluminum which represent spatial and contrast resolution benchmarks. Visualizing a certain hole implies a specific resolution for a given linear accelerator/EPID combination. Properly setup EPIDs will typically be able to resolve the 17 shaded holes in Figure13. Most should be able to resolve another 4 marked with X's. AMFPI systems should be able to resolve all the holes. Shalev and colleagues have introduced a phantom and software tool that allows the user to quantify EPID spatial resolution and contrast to noise ratio (CNR).[88] The software determines CNR and spatial resolution from images acquired of a standardized phantom. The resolution and noise values reported may be used as baseline values for acceptance testing and ongoing QA of the EPID. The user is encouraged to demand this type of quality test at acceptance to help guarantee that the EPID is indeed operating at or above specifications. The spatial resolution indicated in the final row of Table II represents the spatial resolution (in line pairs per mm) for commercial EPID configurations as determined using this phantom and analysis tool.[88] A value of 0.25 indicates 2mm spatial resolution. Regardless of which phantom is used and whether quantitative software

is applied, the initial images represent base line data for continuing quality assurance of the EPID. These should be the best images the system can obtain. In addition, images of anthropomorphic phantoms (phantoms used in a diagnostic radiology department may be better for this purpose than a sliced RANDO phantom) should be stored to represent the operation of

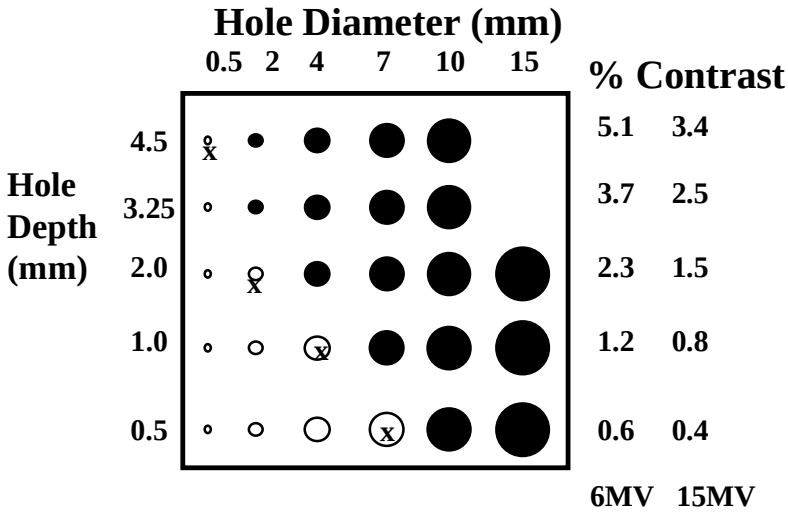

Fig 13 - Aluminum Las Vegas phantom for EPID image contrast and spatial resolution.

the imager at optimum image quality.

Software

Commissioning of software involves testing of features such as EPID/linac control, network connections, storage, archival/retrieval and backup (including compression schemes), security functions and analysis tools. During commissioning, responsibilities for these operations should be assigned.

If an EPID is intended for use in quantitative evaluation of patient setup, commissioning should involve measurement of known setup errors. These measurements should be designed to separate the results into those based on field placement and the location of the phantom in the field. The effects of image processing (e.g. image enhancement and edge detection) on the accuracy of setup analysis should be established. Image processing may affect the results of quantitative reporting.[72]

The commissioning process should include understanding and characterizing the limits of reference image generators (simulators, DRRs, etc.), since field placement errors are determined by comparing portal images to reference images.

A test should be performed to determine the ability of the system to reproduce a null transform on identical images. It is best to use the EPID's own software to compare an image to itself. A number of users should be recruited to use the setup verification tools to assess setup error on the image pair. This also allows the determination of inter and intra-user variation in error detection, which should be established before setting correction thresholds. Typical accuracy for such tests have ranged from 0.5 mm to 2 mm.

A second procedure involves attempting to assess a known transformation. In this case, a reference image of an anthropomorphic phantom can be taken. This image can be transformed

by a known transformation, or the phantom can be moved by a known amount and re-imaged. The measured transformation can then be compared to the expected transformation. Objective assessment of alignment tools can also be performed using a standard image data set.[89]

A complete dry run of a known phantom through the entire treatment process (CT/simulation, planning, reference image generation, initial setup, imaging and setup measurement) allows testing of the proper operation of the EPID system within the confines of department infrastructure. This will allow identification of other potential sources of error, such as laser calibration differences or limits in DRR resolution. It is also advised to attempt to introduce errors into the alignment by rotating the phantom up to 6 degrees and by generating portal images of varying quality relative to a reference image. An accuracy of ±3 mm and ±1º should be achievable. These tests should be performed for images acquired at all four cardinal gantry angles. Dry run procedures also help in training, education and identifying individual responsibilities. Furthermore, the amount of time necessary for intended EPID use is indicated through dry runs.

B. Quality Assurance

To maintain EPID performance, a quality assurance program must be put in place. The program must define specific measurements, frequencies and tolerances (Table IV). Figure 14 shows examples of EPID QA daily and monthly worksheets for a matrix ion-chamber system in clinical use. The QA program should be in writing and records of the completed tasks should be kept for review.

Frequent (e.g. daily) quality assurance procedures include safety features such as mechanical integrity, collision interlocks, etc. Operational and image checks are accomplished by imaging a fixed phantom in a fixed geometry with a given dose. This allows rapid assessment of operability and image quality.

Monthly QA includes detailed safety and mechanical integrity checks (Table IV). A review of daily QA results to determine trends and degradation in image quality should be performed. The interval for re-calibration of the imager is initially determined by the vendor and established at the time of commissioning, and may be changed through observation of trends in image quality. Periodic (e.g. monthly) disk and database maintenance should also be performed.

A rapid check of software performance for quantitative measurement should be performed on an annual basis. This could involve a dry run using an anthropomorphic phantom, or could be performed using a geometric phantom (e.g., a radiosurgery target ball placed in a known location in the room coordinate system). Software QA should also be performed with upgrades and changes in the EPID system.

Figure 14 a) Daily QA, b) Monthly QA

Daily EPID Quality Assurance Log
Dept. of Rad. Onc.
Date: _____ Initials: _____

Collision Interlocks	
Upper Arm: Left Side Panel	❑ Alarm Sounds
Upper Arm: Right Side Panel	❑ Alarm Sounds
Collision Bar	❑ Alarm Sounds
Cassette Head: All 4 Sides & Top	❑ Alarm Sounds

Image Quality

1. Move EPID to P2, place Las Vegas Phantom on cassette surface, and align cross-hairs.
2. Close the jaws to the edge of the phantom.
3. Load patient "Physics - Daily QA" and choose the treatment field corresponding to the day of the week.
4. Acquire an image of the phantom.
5. Window and level the image until holes show up clearly.
6. In the diagram to the right, mark an *X* in the right-hand circle of each row if it is visible in the image.
7. Save the image and record the following information:

Energy (circle one):	6 MV	18 MV
Dose Rate (circle one):	80 MU/min.	400 MU/min.
Acquisition Mode:	Optimum Quality	
Specifications:	Rows marked in diagram are visible in the image for given energy.	

Position Verification		
Move EPID to P2 (138.5 cm at cassette surface) and record the following information:		
	Optical Distance Indicator	Light-Field Cross-Hairs
Measured		
Calibration	138.5 cm	0 mm
Difference		
Tolerance	± 1 cm	± 2 mm

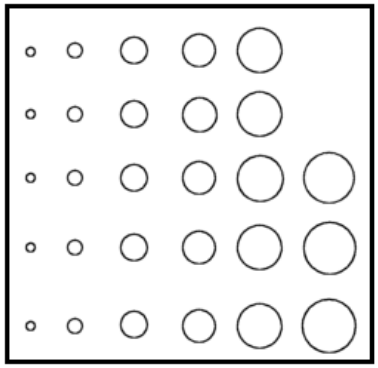

Daily Problem Log	
Problems	Comments / Explanation / Description of Problem
Deployment of R-Arm	
Retraction of R-Arm	
Interlocks	
Image Quality	
Software	
Other	

Monthly EPID Quality Assurance Log
Dept. of Rad. Onc.
Date: _____ Initials: _____

Review of Daily QA Log			
Collision Interlocks	❑ No problems ❑ Problems	If problems occurred, has action been taken and documented in the Maintenance section?	❑ Yes
Position Verification	❑ No problems ❑ Problems	If problems occurred, has the EPID been recalibrated and documented in the Calibration section?	❑ Yes
Image Quality	❑ No problems ❑ Problems	If problems occurred, has the EPID been recalibrated and documented in the Calibration section?	❑ Yes
Daily Problem Log	❑ No problems ❑ Problems	If problems occurred, have the problems been addressed and documented appropriately?	❑ Yes

Collision Interlocks				
	Alarm Sounds	R-Arm Motion Disabled	Couch Motion Disabled	Gantry Motion Disabled
Upper Arm: Left Side Panel	❑	❑	❑	❑
Upper Arm: Right Side Panel	❑			
Collision Bar	❑			
Cassette Head: All 4 Sides & Top	❑			

Contrast and Spatial Resolution

1. Move EPID to P2, place Las Vegas phantom on cassette surface, and align cross-hairs.
2. Close the jaws to the edge of the phantom (approx. 11x11 cm).
3. Load patient "Physics - Monthly_QA" and choose the treatment field corresponding to the desired energy / dose rate combination.
4. Acquire an image of the phantom.
5. Window and level the image until holes show up clearly.
6. Save the images and record the information in the table below.

If the contrast resolution (determined by the rows visible) or the spatial resolution (determined by the columns visible) do not meet tolerances, image acquisition recalibration may be necessary.

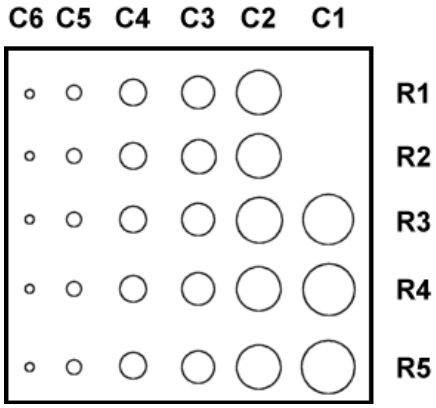

Energy / Dose Rate	Row Visible	Row Tolerance	Column Visible	Column Tolerance
6 MV / 80 MU/min.		R4		C5
6 MV / 400 MU/min.		R4		C5
18 MV / 400 MU/min.		R3		C4

Image Statistics

1. Move EPID to P2 and set the collimator jaws to the edges of the detector.
2. Load patient "Physics - Monthly_QA" and choose the treatment field "Flood Field."
3. Acquire a flood field image.
4. When the image comes up, choose "View —> Measure —> Histogram".
5. Choose "ROI" to be "Full Image" and record the values found under "Pixel Statistics" below:

	Max - Min	Mean	N
Measured			
Tolerance	< 60	N/A	< 0.8%

If any value exceeds tolerance, repeat image acquisition. If tolerance is still exceeded, recalibrate.

Position Verification

Move EPID to P2 (138.5 cm at cassette surface) and record the following information:

	Optical Distance Indicator	Centering of Cross-Hairs
Measured		
Accepted	138.5 cm	0 mm
Tolerance	± 1 cm	± 2 mm

If either exceeds tolerance, conduct a mechanical recalibration and repeat position verification. Mechanical recalibration may also require image acquisition recalibration.

Troubleshooting

	OK	Not OK
Horizontal Lines (thin): Consistent presence indicates need for recalibration.	❑	❑
Vertical Lines (thin): Consistent presence indicates faulty electrodes; replace detector.	❑	❑
Dose Bars (thick horizontal): Consistent presence indicates linac dose instability.	❑	❑
Bubbles: Indicates presence of air in chamber or compression of chamber; recalibrate.	❑	❑
R-Arm Motion: Jerky motion might indicate imminent failure of motor or drive controller.	❑	❑
Hand Pendant: Consistent loss of signal may indicate a failing battery.	❑	❑

Calibration

❑	Mechanical recalibration performed & recorded in the "Maintenance" section.
❑	Image acquisition recalibration performed & recorded in the "Calibration" section.

V. CLINICAL APPLICATION OF EPIDs

The primary applications of EPID include verification of patient setup and assessment of target and organ motion. Current research includes use of EPIDs for compensator design and verification, treatment machine QA and patient dosimetry.

A. Preparing for EPID implementation

Certain specific goals and protocols for the use of EPIDs must be established *before* they can be successfully brought into the clinic.[90,91] Table V lists examples of questions that should be discussed before EPID implementation. Table VI shows estimates of physician, therapist and physicist time to implement a simple EPID program. It should be noted that EPID use and responsibilities differ between clinics around the world and between different EPIDs and these tables are guides indicative of issues each clinical team should address.

B. Software Tools

The complexity of EPID software has evolved over the past decade in response to improved understanding of clinical applications as well as flexibility of acquisition modes for new EPID technology.

Image Acquisition

A typical portal imaging system will have a user interface that allows selection of different image acquisition modes. Although the range of operating modes may vary, the following are commonly available on commercial EPIDs:

Single exposure (localization): In this mode of acquisition, a single image is acquired for a short period of time (typically at the start of the treatment). The duration of the exposure can either be controlled by a fixed time criterion or by the time that the beam is on.

Verification image: Verification images can either be an average of multiple images acquired during a period of treatment, or single images acquired over a longer period of time (higher dose) than the localization images mentioned above.

Double exposure: This mode of operation is similar to that of weekly portal film acquisition. One image is the single exposure image, and the second is an "open field" image. Again, control of each image acquisition may be via fixed time intervals or by the duration of the beam. Typically, the open field and portal images are combined using a weighted sum to produce a single image. A field outline from the portal can also be automatically extracted and overlaid on the open field image.

Movie-loops: The digital nature of the EPID allows movie loops or on-line fluoroscopy to be acquired during treatment. In some cases, all of the images mentioned above are generated by summation of one or more images acquired in a loop.

Image Enhancement Tools

Once an image has been acquired, unlike film, the image data can be manipulated to improve landmark visibility and image interpretation. Simple and sometimes automatic image enhancement tools are available on all EPIDs, giving a major advantage over film

One class of enhancement tools adjusts portal image contrast. The most basic of these, global contrast enhancement, involves manipulation of the gray scale lookup table of the video monitor displaying the image. The window and level values determine what pixel values are

displayed and the range of video intensity values that these are mapped to. This method is typically interfaced to the user by 'slider' bars adjacent to the image.

More advanced techniques employ non-linear mappings of pixel values within the image based on redistributing intensity values to normalize the shape of the intensity histogram. These histogram equalization techniques alter a pixel's intensity based on the global or local adaptive histogram equalization (AHE) distribution of intensity. A disadvantage of AHE is the fact that the procedure is non-linear, causing distortions of anatomical structures and field edges, which could affect quantitative measurement.[92,93]

High pass filtering can also achieve feature enhancement within a portal image, and can be performed by the convolution of a filter kernel and image to produce the feature enhanced image.[94] Typical kernels include the Sobel (first derivative) and Laplacian (second derivative of the image) filters. A third known as an unsharp mask involves subtracting a smoothed version of the image from the original, removing all low frequency components.[95] This processed image is combined in a weighted sum with the unprocessed image. Filtering can also be performed in the frequency domain by first calculating the Fourier transform of the image and applying a filter function to the image.[96] Calculating the inverse transform of the result generates the filtered image.

A disadvantage of high pass filtering is the effect of noise amplification caused by the operation of the high pass filter. A compromise can be found by the application of a Weiner filter that produces the most optimal reconstruction of the image based on a least squares minimization criterion.[97] There is no single "best" enhancement scheme. Enhancement schemes should be selected by the users for the sites and image acquisition modes to be used clinically.

Setup Verification / Error Detection Tools

Treatment setup verification can be divided into verification of the geometric configuration of the treatment unit, and verification of the patient and target position with respect to the treatment geometry.

Proper evaluation of treatment setup involves relating the information in a portal image to that extracted from a reference "gold standard" of treatment setup. The gold standard information can be a reference radiograph (simulation film or DRR), features extracted from the reference image (e.g., the field border and the anatomic landmark information), or three-dimensional models of the patient (e.g., CT data).

Digital measurement tools such as digital rulers can determine the distance from a given field border to critical projected anatomic interfaces. While not providing complete information on the nature of patient setup, such tools may be used for rapidly assessing critical features of daily setup such as field centering or spinal cord avoidance.

More detailed information about patient setup can be accomplished through the use of image registration algorithms. These can be classified loosely by the general mechanism used for selecting an optimal transformation.

Landmark based techniques use geometric description of landmarks to determine a transformation that aligns a reference and portal image. Landmark descriptions that have been used include points, open curves, and drawn templates.

If points can be precisely localized, they can be aligned with high precision. The major difficulty with the use of point landmarks is the lack of suitable points. Observation of typical radiographs indicates very few internal anatomic regions that can be precisely localized as points on projections. Projections of external fiducial marks have been used as point landmarks, but

these points may not properly reflect patient setup errors. Implanted fiducials have also been investigated for use in reproducible setup of the head. It is important to assess the reproducibility of selected point landmarks.

A large number of anatomic landmarks can be described adequately as open curve or line segments. A template-matching algorithm allows a user to draw an arbitrary set of landmarks on the reference image, and to determine an optimal transformation for alignment by manually shifting these landmarks until they are properly overlaid on the portal image.[98] This system can be very fast, permitting on-line use. Other curve matching tools are more automated, providing the optimal transformation by determining the transform that best aligns overlapping curve segments.[99]

The use of landmark-based alignment algorithms requires a trained user to spend time to identify landmarks for use in alignment. Contrast based algorithms show some promise for fully automated alignment. Typically, the intensity distribution in a region of a reference image is defined as a template. Using cross-correlation techniques, the transformation that optimally matches this template to a corresponding intensity distribution in the portal image is found.

Such techniques have been implemented to align whole images,[100] and to select point landmarks based on the alignment of a series of small regions of interest containing distinct gray level distributions.[101] An important consideration for contrast based alignment techniques is the source of reference and setup radiographs. In order for most contrast based algorithms to perform optimally, both images involved should have similar contrast distributions. Simulator-produced images have different contrast than portal images due to the different absorption and scatter properties inherent with different energies of radiation. Solutions to this problem have been to establish a "gold standard" portal image at the beginning of treatment, or to optimize the DRR generation algorithms to produce contrast similar to that found in megavoltage radiographs.[89,102]

Modern image processing techniques take advantage of the ability of computers to identify features in an image using properties similar to those a human observer is believed to use. Gilhuijs and colleagues developed a procedure for automated extraction of anatomic features and alignment to a user-defined set of reference landmarks.[103] In this procedure, a top hat transformation was used to extract a set of candidate coordinates for locations of bone-soft tissue interfaces. The optimal transformation that aligns the reference and portal anatomy is determined by chamfer matching of these coordinates with the distance space determined from the manually defined reference landmarks. Fritsch and colleagues have made significant progress in the application of computer vision techniques to the problem of image registration in radiotherapy.[104] Using the multiscale medial axis filter, they have developed a system that extracts "cores" from radiographs. These cores are three-dimensional descriptions of features in images. Two of the dimensions are used to indicate the location of object "middles", and the third describes the object's width at the given location. Such features have been evaluated for use in image alignment with promising results.[103,104]

Field edge detection is another important concern. There are two reasons to find the radiation field on the image. As most imagers do not maintain a rigid and reproducible relationship with respect to the central axis of the treatment unit, the location of the radiation field can be used to establish a coordinate system within which the variation of the location of patient anatomy can be determined. In the absence of a shaped radiation field, or when a field extends beyond the borders of the image, a graticule projection may also serve this purpose. A

second important role for portal field border extraction is verification of the shape and orientation of the treatment portal.

A number of investigators have developed means of extracting the radiation field borders from portal images automatically.[105-107] The intensity histogram from a portal image typically has two distinct peaks, representing the area outside the radiation field, and the pixels within the field. The range of pixel values between these peaks represents the beam penumbra. A reasonable threshold can be extracted automatically from this histogram to track the field borders. When a field border is in air, or near a rapidly changing density region of the patient, this technique may run into difficulty. Bijhold and colleagues developed a tracking algorithm that overcomes some of the limitations of threshold based field border extraction.[105] McGee developed a system to track the consistency of the field borders based on a model extracted from the initial treatment field. Wang and Fallone have developed a mathematical model for local field penumbra extraction.[108]

One significant limitation of much of the setup error analysis done to date is that the majority of clinical evaluation tools are based on two-dimensional (2D) analysis of portal images. An interactive procedure to quantify the setup variation of the patient in 3D, based on fast computation of digitally reconstructed radiographs (DRRs) in two beam directions, has been developed. Computer aided comparison of these DRRs with corresponding portal images produces patient setup error information in 3D.[109-112]

C. EPID CLINICAL USE

The types of errors detected include field and block shape errors and field or patient placement errors. There are two general methodologies in using an EPID for patient setup verification and correction; on-line or off-line (Figure 15). For on-line correction, a pre-treatment port can be acquired and evaluated such that any setup error will be corrected before the treatment continues. First day portal film localization is an example of an on-line correction.

Fig 15 – Schematic of on-line and off-line correction approaches

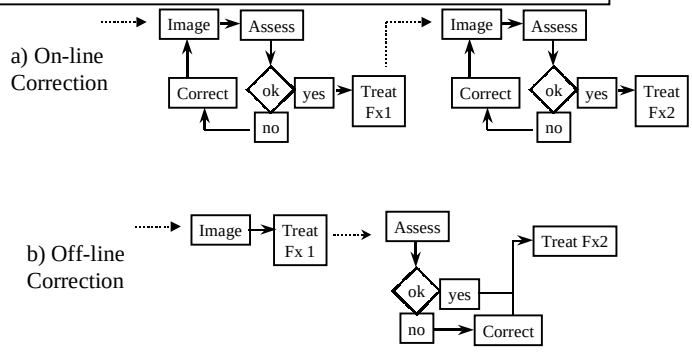

The most basic manifestation of off-line correction occurs when the portal image is examined after treatment and, if necessary, a correction is made at the following treatment session. Standard weekly port films are an example of this strategy. Off-line correction has also evolved into strategies whereby multiple periodic images are evaluated to improve statistical certainty for one or more corrections over an entire treatment session.

EPID Clinical Protocol (step by step)

The following describes a simple procedure for using the EPID in the clinic. 1)For each patient, enter patient demographic, field data. Image acquisition data is also entered, e.g. single or double

exposure, movie-loop, etc. The type and amount of data necessary varies depending on the EPID manufacturer. If the EPID is part of an integrated information system, much of the data input is done automatically when the treatment course is initially setup. 2) At treatment time, the EPID is put into imaging position, the patient is selected, the field is selected and acquisition parameters loaded. Again, if the EPID becomes more integrated into the treatment system, the information system will automatically download the EPID with correct data for that patient and field. 3) Image the patient and take action as the protocol directs. The action may include doing nothing, performing on-line or off-line setup correction. If the EPID is part of the information system, recording, storing and retrieving the image may be simplified.

On-line EPID use

An early group of on-line EPID studies involved taking prospective action based on a pre-treatment port. This type of protocol has been implemented in a number of centers and allows the reduction of both random and systematic errors for each individual patient, but does not differentiate between systematic and random error.[9,17,18,113] Results of these studies indicate that up to 50% of initial fields are judged in error and corrected. The error correction rate is anatomical site dependent and due to the visual analysis, observer dependent as well. While improvement in setup accuracy was noted in these studies, final off-line analysis shows that some residual setup error remained. An example of on-line setup correction and final error is shown in Figure 16.[17] Visual analysis is not quantitative and as shown in Figure 16, even after correction, quantitative off-line analysis found that 15% of setups were still in error by more than 5mm. In addition, these studies depend primarily on two-dimensional analysis and manual patient setup correction can increase treatment time. For these reasons, daily on-line EPID imaging is not practiced in many centers. There are however examples of on-line correction strategies in use today, where the clinicians feel that the additional time to make a correction is warranted.[114]

Fig 16 – Visual On-Line correction

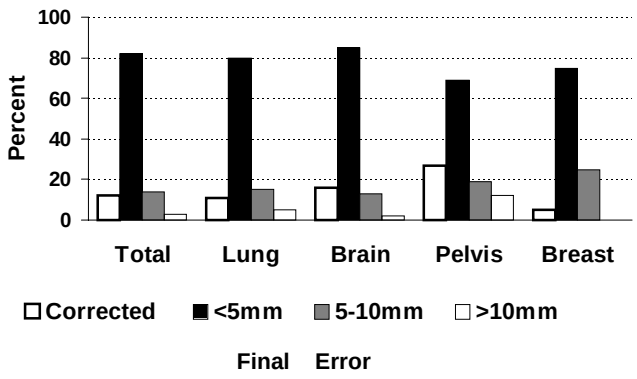

More quantitative daily correction approaches have been developed, which utilize automated image analysis tools, developed commercially or in-house, to substantially increase accuracy, with modest increase in effort. A computer-aided on-line analysis and correction system has been implemented to correct pelvic and thoracic treatment setup errors daily.[21,24,26,27,98] While these studies showed a significant improvement in setup accuracy, additional treatment time or personnel may be required, due to the need to analyze images and adjust patient setup. The computerized nature of the EPID allows it to be integrated into a larger scale decision-making system. Such an integrated system can help the users decide when it is appropriate to make a correction and when not to, based on the established physician and treatment planning guidelines.[115] The quest for improved efficiency and automation in the use of EPIDs is ongoing and pursued both by research groups and vendors.

Off-Line EPID use

Off-line EPID models can be separated into three groups, simple off-line correction (film model), monitoring and statistical decision models.

Simple Off-line:The simplest use of the EPID is to replace weekly portal filming, where the EPID is used to generate hard copy as with film (Fig 15b).[116] The EPID also provides additional benefits compared to film; faster imaging time and image enhancement (e.g., contrast enhancement, edge enhancement) algorithms can be applied immediately. Error detection can be accomplished manually, with computer assistance in an interactive mode, or automatically.

Monitoring: The earliest clinical EPID studies were of the monitoring type, where images are acquired, but no action is taken. Lam described the frequency and magnitude of field placement errors (FPE) in thoracic and abdominal radiotherapy, suggesting that errors exceeding conventional planning margins may not be uncommon.[117] Others have created summary data showing the cumulative effect of daily FPE on the course of radiotherapy for individual patients[118] and then extended the methodology to indicate the effects of FPE on treated doses.[119] This strategy has also been utilized to determine time trends in patient setup accuracy, showing that patient setup error can increase during the course of therapy and that routine imaging is essential to maintain accurate treatment.[120]

Movie loops have been used to monitor target and normal tissue motion between and during treatment fractions during tangential breast field treatment.[7,16,121] The comprehensive analysis enabled by EPID use shows the magnitude and frequency of setup and motion errors for a group of patients and more importantly for individual patients. An example of motion of the lung-chest wall interface seen through 6-7 images during each treatment fraction is shown in Figure 17, indicating the wide range of motion that occurs due to respiration during treatment.[122] Daily and weekly imaging samples are also indicated in the figure (W). It is clear that weekly portal imaging can not be used to quantify tissue motion due to respiration, which can exceed 2 cm during tangential breast treatments.[22]

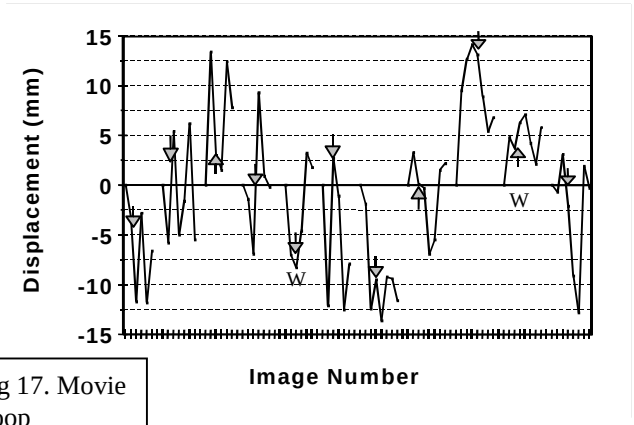

Fig 17. Movie Loop

Prostate motion studies using radio-opaque markers show that while the prostatic tissue relative to bony pelvis does not move appreciably during treatment, it can move over 1.5cm relative to the bones between fractions.[123] Other pelvic setup studies show that setup errors exceeding 1 cm were not uncommon, and that these inter-treatment values exceed any intra-fractional motion errors for the pelvis.[124]

Statistical models/decision rules:

Statistical models have evolved to allow treatment verification for complex treatments without a large increase in time or cost for the information. Two examples are presented.

Decision Rule example 1 (analysis based on a global standard): A systematic error correction protocol based on establishing error thresholds derived from a patient population for a

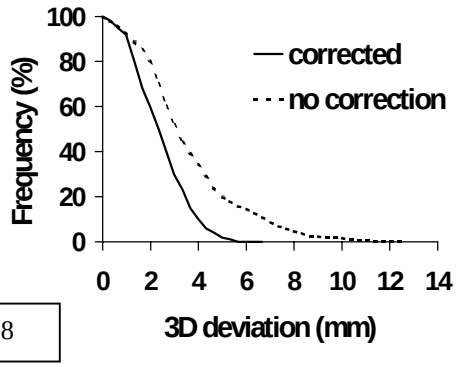

Fig 18

specific treatment site has been discussed.[20,23,32] The need to correct systematic error for any patient is evaluated with respect to this institutional or global threshold. These studies have demonstrated that reduction of systematic error of approximately a factor of 2 (compared to uncorrected) is achievable, with an average of less than 10 images and approximately 0.5 corrections per patient treatment course (Figure 18). In other words, with about the same imaging effort as film, and the tools of the EPID, significant error reduction can be achieved.

Decision rule example 2 (analysis based on an individual standard): The ability to gather enough data to make systematic and random error assessment on individual patients with EPID has also been introduced. In the population - based correction models, the setup errors are assessed for all patients (plotted in Figure 19a). If an EPID is used to acquire daily portal images for individual patients, then the data in Figure 19a can be replotted in Figure 19b as the average setup variation for each of 25 pelvic patients. Clearly, the margin of 11 mm (arrow) is unnecessarily large for an appreciable number of the patients, and yet inadequate for 2 patients. The data also suggest that some patients are highly reproducible in their daily setup. Individual treatment margins can be re-optimized for a specific margin reduction so that a higher dose might be delivered.

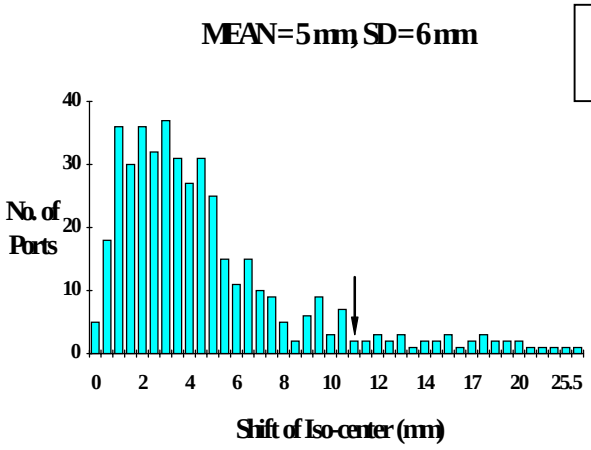

Fig 19
A B

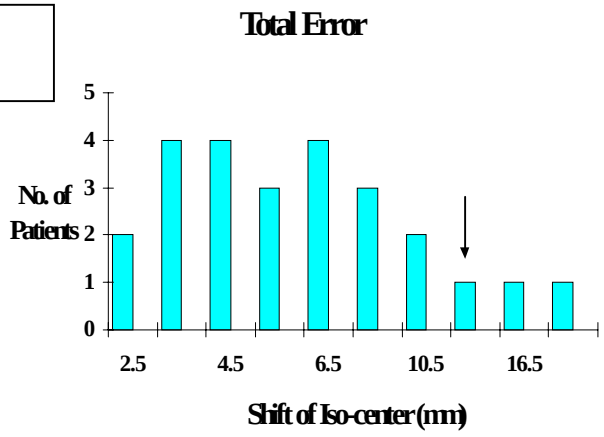

The concept of Adaptive Radiation Therapy (ART) has been introduced by Yan et al. as a closed-loop feedback process for correction of the individual patient setup error.[125,126] Extending the idea by Denham[127] on the optimal frequency to take daily portal images, the nature of treatment variations are characterized for a few fractions early in the course of treatment such that they can be confidently estimated for the remaining course of treatment. This allows for the application of patient specific treatment corrections. Similar work in the use of EPID for early error detection and correction for dose escalation protocols is also underway.[128]

There are additional recent examples of off-line and statistical analysis.[129,130]

D. Advanced Applications

Treatment QA

The EPID has also been put to use for quality assurance of treatment machines[86,131,132] and of treatment techniques, such as radiosurgery[133] and dynamic treatment delivery.[134-136] Investigators have used the EPID for the design[137-140] and verification[141-143] of compensating filters. EPIDs have also been employed in the verification and QA of intensity modulated treatments[136,144-146] and gated treatments.[68] In each case, the EPID has allowed more precise, quantitative results to be obtained with much less effort than would have been achievable using conventional QA tools.

Exit Dosimetry

More recently, there has been much interest in determining *in vivo* dose distributions during treatment with an EPID. While setup error and patient motion are quantified with EPID imaging, the ultimate value of concern is dose to target and normal tissue. Efforts to determine and quantify dose in two and three dimensions are underway. The earliest works investigated the characteristics of the various EPIDs for transmission dose measurement.[67,87,147-149] These studies indicate that with the proper calibration and care, the EPID can be used to generate an exit dose image and values that are within 2-5% of expected values. Much additional work has gone into the interpretation of the EPID image in terms of a quantitative exit dose and implications for dose at the target.[74,145,150-161] It should be noted that there may be significant differences related to quality control and calibration problems in determining dose with an EPID and extreme caution should be used.

VI. Cost and Future

A. Cost

The major expense for an EPID is the initial cost ranging from $80,000 to $350,000 (in 2001). The comparable initial expense for film portal imaging is about $25,000. However, the ongoing costs for film portal imaging are substantial, where the EPID ongoing equipment and per image costs are almost negligible. The extra amount of time and labor needed to process film and display it for review is expensive, but varies depending on location and who performs the work. It has been shown that for large centers, or even smaller centers that image frequently, EPIDs can be more cost effective than film.[162] It is therefore expected that with more frequent use, an EPID should be more economical than film.

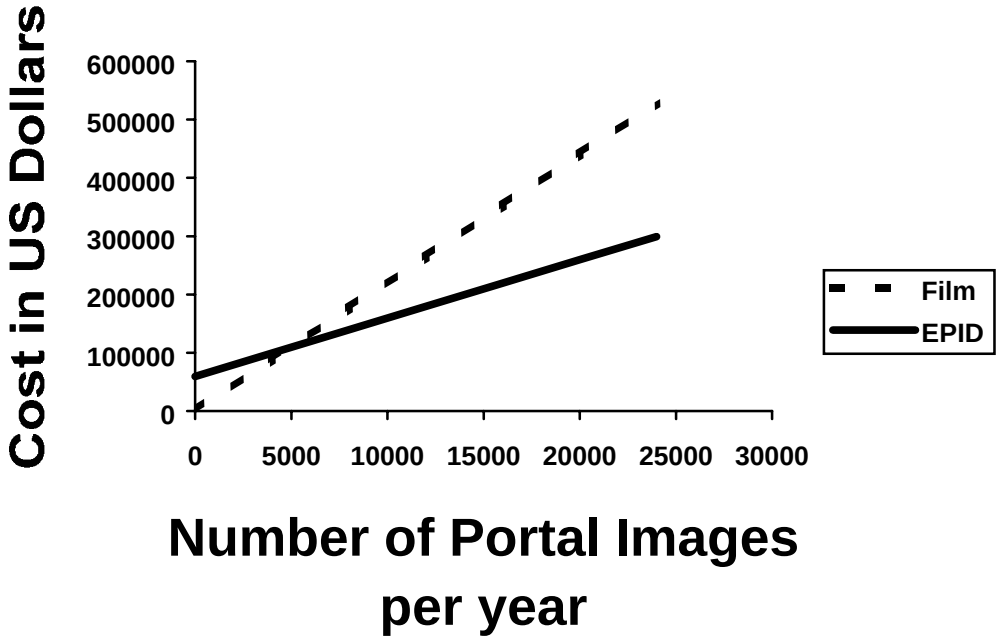

Figure 20 shows changes in total annual cost of imaging with film and EPID as a function of increasing use of portal imaging based on the usage model of a TG58member. The absolute numbers on each axis need to be adjusted for individual situations. The graph shows clearly that if portal imaging is performed frequently, then EPID is less expensive to use than film. Analyses such as these must consider capital costs, annual maintenance, and personnel time. It is important to note that this cost analysis treats EPID and film as identical in clinical value, ignoring the fact that the EPID is far more powerful than film for error analysis and in some cases can do things that can not be done with film. Quantifying personnel costs specific to expected utilization of an EPID will help assess the economic impact of EPID use. The choice of correction strategy of any EPID protocol has the most direct impact on the allocation of personnel and computer resources. Table VII lists estimates of the necessary resources to implement various correction strategies. These estimates are based on imaging all patients at 2.5 fields per patient. Four strategies are distinguished. The first column pertains to the simplest strategy where images are inspected visually on-line to prevent gross error. The tolerance for correction should be set large so as not to impede treatment throughput but also to avoid erroneous correction. Images are not archived for analysis and the strategy incurs minimal cost. The second column presents perhaps the most complex and sophisticated use of the EPID where setup error is assessed and corrected on a daily basis. This strategy corrects for both systematic and random error, and in theory, should achieve the highest accuracy. However, this strategy can also be most costly in terms of time and effort. The third column is for an off-line correction strategy that is similar to the weekly port film practice. Additional software and hardware options can be very helpful. The final column represents the off-line strategy that is based on statistical decision models. The approach requires the commitment of personnel and computer resources to archive and analyze the data, but also provides the potential for reduction of effort at the treatment unit. For example, field placement error can be corrected by moving a multi-leaf collimator via network. Note that the associated resource costs stated for the four strategies are estimates of total cost. This should be compared

to film imaging (similar to column off-line (a)). For larger departments, some economy of scale should be expected.

B. Future

New flat panel AMFPI detectors will soon be mainstream from all vendors. This will provide simple and high quality imaging that will prove to be essential for verification and quality assurance in the use of high technology radiation therapy. New methods will continue to be developed to apply EPIDs effectively in clinical practice.

It is very important to note that the data infrastructure and the clinical utilization process must be understood to fully take advantage of any new or advanced technology.

VII. SUMMARY AND RECOMMENDATIONS

The TG58 report was written to enhance the knowledge of the medical physicist in implementing EPID technology in the clinic. From reading this report, the reader should understand:

1. The basic physical principles of image formation and megavoltage imaging. This provides the reader with the essential background necessary to understand the function, limitations and quality assurance of EPID systems.
2. The technical and practical manifestations of the megavoltage imagers. This gives the reader an understanding of the hardware, software and production characteristics of commercially available systems. Critical components related to image quality, EPID operation, performance and safety are indicated and must be understood for optimal clinical use.
3. Details of installation, commissioning and developing and performing continuing quality assurance. Essential characteristics to consider and steps to be taken to bring EPID technology into the clinic, verify proper operation and establish a viable quality assurance program are provided.
4. Critical questions that should be discussed to help the reader prepare for the purchase, installation and continuing effective use of an EPID. This includes understanding the clinical situation and potential resource commitments.
5. Availability and operation of various image acquisition, enhancement and analysis software to make appropriate equipment selection and specifications.
6. The models of successful clinical EPID use, which demonstrate a wide variety of application from simple to sophisticated. Reading these references provides detailed information on the cost, benefit and implementation of each EPID protocol.
7. How to establish costs for EPID implementation, from capital equipment to human resources. Choice of clinical application has a strong influence on total costs.
8. That the technology for EPID is changing and improving. Any purchase should consider upgrades in both software and hardware.

This task group recommends that:

- The medical physicist become familiar with the physics of megavoltage portal imaging (Section II) and its commercial manifestations (Section III). This information allows the reader to establish clear specifications and to maintain an effective EPID.
- The medical physicist understand the details of the installation, commissioning and the QA process of an EPID (Section IV). Only if these issues are understood can the physicist be prepared to bring the EPID system into the clinic and maintain the system at optimum performance.

- The treatment team evaluate the tables in Section V regarding clinical use, resource commitment and education. Since each clinical use of EPID may be different, evaluating these issues before selecting and implementing an EPID is paramount.
- The medical physicist evaluate ongoing education, upgrades and clinical uses of EPID to remain knowledgeable in maintaining and improving the quality of EPID application.

Acknowledgements - The authors wish to thank all of our clinical colleagues that have provided input and discussion on the use of EPID.

References

[1]J. E. Marks, A. G. Haus, H. G. Sutton and M. L. Griem, "Localization error in the radiotherapy of Hodgkin's disease and malignant lymphoma with extended mantle fields," Cancer **34** (1), 83-90 (1974).
[2]I. Rabinowitz, J. Broomberg, M. Goitein, K. McCarthy and J. Leong, "Accuracy of radiation field alignment in clinical practice," Int. J. Radiat. Oncol. Biol. Phys. **11** (10), 1857-67 (1985).
[3]S. A. Rosenthal, J. M. Galvin, J. W. Goldwein, A. R. Smith and P. H. Blitzer, "Improved methods for determination of variability in patient positioning for radiation therapy using simulation and serial portal film measurements [see comments]," Int. J. Radiat. Oncol. Biol. Phys. **23** (3), 621-5 (1992).
[4]J. M. Balter, H. M. Sandler, K. Lam, R. L. Bree, A. S. Lichter and R. K. ten Haken, "Measurement of prostate movement over the course of routine radiotherapy using implanted markers," Int. J. Radiat. Oncol. Biol. Phys. **31** (1), 113-8 (1995).
[5]S. E. Griffiths, R. G. Pearcey and J. Thorogood, "Quality control in radiotherapy: the reduction of field placement errors," Int J Radiat Oncol Biol Phys **13**, 1583-8 (1987).
[6]H. Huizenga, P. C. Levendag, P. M. De Porre and A. G. Visser, "Accuracy in radiation field alignment in head and neck cancer: a prospective study," Radiother. Oncol. **11** (2), 184-7 (1988).
[7]G. van Tienhoven, J. H. Lanson, D. Crabeels, S. Heukelom and B. J. Mijnheer, "Accuracy in tangential breast treatment set-up: a portal imaging study," Radiother. Oncol. **22** (4), 317-22 (1991).
[8]C. Mitine, A. Dutreix and E. van der Schueren, "Tangential breast irradiation: influence of technique of set-up on transfer errors and reproducibility," Radiother. Oncol. **22** (4), 308-10 (1991).
[9]A. Ezz, P. Munro, A. T. Porter, J. Battista, D. A. Jaffray, A. Fenster and S. Osborne, "Daily monitoring and correction of radiation field placement using a video-based portal imaging system: a pilot study," Int. J. Radiat. Oncol. Biol. Phys. **22** (1), 159-65 (1992).
[10]J. Bijhold, J. V. Lebesque, A. A. Hart and R. E. Vijlbrief, "Maximizing setup accuracy using portal images as applied to a conformal boost technique for prostatic cancer," Radiother. Oncol. **24** (3), 261-71 (1992).
[11]C. Weltens, G. Leunens, A. Dutreix, J. Cosset, F. Eschwege and E. van der Schueren, "Accuracy in mantle field irradiations: irradiated volume and daily dose," Radiother. Oncol. **29** (1), 18-26 (1993).
[12]C. Mitine, A. Dutreix and E. van der Schueren, "Black and white in accuracy assessment of megavoltage images: the medical decision is often grey," Radiother. Oncol. **28** (1), 31-6 (1993).
[13]P. B. Dunscombe, K. Fox, S. Loose and K. Leszczynski, "The investigation and rectification of field placement errors in the delivery of complex head and neck fields," Int. J. Radiat. Oncol. Biol. Phys. **26** (1), 155-61 (1993).
[14]P. Dunscombe, S. Loose and K. Leszczynski, "Sizes and sources of field placement error in routine irradiation for prostate cancer," Radiother. Oncol. **26** (2), 174-6 (1993).
[15]M. A. Hunt, G. J. Kutcher, C. Burman, D. Fass, L. Harrison, S. Leibel and Z. Fuks, "The effect of setup uncertainties on the treatment of nasopharynx cancer," Int. J. Radiat. Oncol. Biol. Phys. **27** (2), 437-47 (1993).
[16]C. L. Creutzberg, V. G. Althof, H. Huizenga, A. G. Visser and P. C. Levendag, "Quality assurance using portal imaging: the accuracy of patient positioning in irradiation of breast cancer," Int. J. Radiat. Oncol. Biol. Phys. **25** (3), 529-39 (1993).
[17]M. G. Herman, R. A. Abrams and R. R. Mayer, "Clinical use of on-line portal imaging for daily patient treatment verification," Int. J. Radiat. Oncol. Biol. Phys. **28** (4), 1017-23 (1994).
[18]J. Gildersleve, D. P. Dearnaley, P. M. Evans, M. Law, C. Rawlings and W. Swindell, "A randomised trial of patient repositioning during radiotherapy using a megavoltage imaging system," Radiother. Oncol. **31** (2), 161-8 (1994).
[19]M. A. Hunt, T. E. Schultheiss, G. E. Desobry, M. Hakki and G. E. Hanks, "An evaluation of setup uncertainties for patients treated to pelvic sites," Int. J. Radiat. Oncol. Biol. Phys. **32** (1), 227-33 (1995).
[20]A. Bel, R. Keus, R. E. Vijlbrief and J. V. Lebesque, "Setup deviations in wedged pair irradiation of parotid gland and tonsillar tumors, measured with an electronic portal imaging device," Radiother. Oncol. **37** (2), 153-9 (1995).
[21]F. Van den Heuvel, W. De Neve, D. Verellen, M. Coghe, V. Coen and G. Storme, "Clinical implementation of an objective computer-aided protocol for intervention in intra-treatment correction using electronic portal imaging," Radiother. Oncol. **35** (3), 232-9 (1995).
[22]A. Lirette, J. Pouliot, M. Aubin and M. Larochelle, "The role of electronic portal imaging in tangential breast irradiation: a prospective study," Radiother. Oncol. **37** (3), 241-5 (1995).

[23]A. Bel, P. H. Vos, P. T. Rodrigus, C. L. Creutzberg, A. G. Visser, J. C. Stroom and J. V. Lebesque, "High-precision prostate cancer irradiation by clinical application of an offline patient setup verification procedure, using portal imaging [see comments]," Int. J. Radiat. Oncol. Biol. Phys. **35** (2), 321-32 (1996).
[24]J. Van de Steene, F. Van den Heuvel, A. Bel, D. Verellen, J. De Mey, M. Noppen, M. De Beukeleer and G. Storme, "Electronic portal imaging with on-line correction of setup error in thoracic irradiation: clinical evaluation," Int. J. Radiat. Oncol. Biol. Phys. **40** (4), 967-76 (1998).
[25]R. Halperin, W. Roa, M. Field, J. Hanson and B. Murray, "Setup reproducibility in radiation therapy for lung cancer: a comparison between T-bar and expanded foam immobilization devices," Int. J. Radiat. Oncol. Biol. Phys. **43** (1), 211-6 (1999).
[26]L. Pisani, D. Lockman, D. Jaffray, D. Yan, A. Martinez and J. Wong, "Setup error in radiotherapy: on-line correction using electronic kilovoltage and megavoltage radiographs," Int. J. Radiat. Oncol. Biol. Phys. **47** (3), 825-39 (2000).
[27]A. Bel, O. Petrascu, I. Van de Vondel, L. Coppens, N. Linthout, D. Verellen and G. Storme, "A computerized remote table control for fast on-line patient repositioning: implementation and clinical feasibility," Med Phys. **27** (2), 354-8 (2000).
[28]J. E. Marks, A. G. Haus, H. G. Sutton and M. L. Griem, "The value of frequent treatment verification films in reducing localization error in the irradiation of complex fields," Cancer **37** (6), 2755-61 (1976).
[29]S. C. Taborsky, W. C. Lam, R. E. Sterner and G. M. Skarda, "Digital imaging for radiation therapy verification," Proc.SPIE **314**, 164-171 (1981).
[30]N. A. Baily, R. A. Horn and T. D. Kampp, "Fluoroscopic visualization of megavoltage therapeutic x ray beams," Int. J. Radiat. Oncol. Biol. Phys. **6** (7), 935-9 (1980).
[31]A. Bel, M. van Herk and J. V. Lebesque, "Target margins for random geometrical treatment uncertainties in conformal radiotherapy," Med Phys. **23** (9), 1537-45 (1996).
[32]J. V. Lebesque, P. Remeijer, van Riel, P. V. Vos, J. C. J. de Boer, A. G. Visser, E. van Lin and S. Feenstra, "Clinical Evaluation of Setup Verification and Correction Protocols: Results of Multicentre Studies of the Dutch Cooperative EPID Group," The Fifth International Electronic Portal Imaging Workshop **Phoenix, AZ**, 20 (1998).
[33]J. W. Motz and M. Danos, "Image information content and patient exposure," Med Phys. **5** (1), 8-22 (1978).
[34]D. W. Rogers, "Fluence to dose equivalent conversion factors calculated with EGS3 for electrons from 100 keV to 20 GeV and photons from 11 keV to 20 GeV," Health Physics **46** (4), 891-914 (1984).
[35]K. Doi, G. Holje, L.-N. Loo, H.-P. Chan, J. M. Sandrik, R. J. Jennings and R. F. Wagner, "MTF's and Wiener Spectra of Radiographic Screen-Film Systems," Bureau of Radiological Health. HHS Publ. 82, 81-87 (1982).
[36]B. Wowk and S. Shalev, "Thick phosphor screens for on-line portal imaging," Med Phys. **21** (8), 1269-76 (1994).
[37]R. Swank, "Measurement of absorption and noise in an x-ray image intensifier," J.Appl.Phys **45**, 3673-78 (1974).
[38]P. Munro, "Imaging with High energy radiation beams," Ph.D. Thesis, (1990).
[39]P. Munro, J. A. Rawlinson and A. Fenster, "Therapy imaging: a signal-to-noise analysis of a fluoroscopic imaging system for radiotherapy localization," Med Phys. **17** (5), 763-72 (1990).
[40]P. Munro, J. A. Rawlinson and A. Fenster, "Therapy imaging: a signal-to-noise analysis of metal plate/film detectors," Med Phys. **14** (6), 975-84 (1987).
[41]J. P. Bissonnette, I. A. Cunningham, D. A. Jaffray, A. Fenster and P. Munro, "A quantum accounting and detective quantum efficiency analysis for video-based portal imaging," Med Phys. **24** (6), 815-26 (1997).
[42]P. Munro, J. A. Rawlinson and A. Fenster, "A digital fluoroscopic imaging device for radiotherapy localization," Int. J. Radiat. Oncol. Biol. Phys. **18** (3), 641-9 (1990).
[43]M. Ishida, K. Doi, L. N. Loo, C. E. Metz and J. L. Lehr, "Digital image processing: effect on detectability of simulated low-contrast radiographic patterns," Radiology **150** (2), 569-75 (1984).
[44]R. T. Droege, "A megavoltage MTF measurement technique for metal screen-film detectors," Med Phys. **6** (4), 272-9 (1979).
[45]P. Munro, J. A. Rawlinson and A. Fenster, "Therapy imaging: Limitations of imaging with high energy x-ray beams," Proc.SPIE **767**, 178-184 (1987).
[46]M. van Herk and H. Meertens, "A matrix ionisation chamber imaging device for on-line patient setup verification during radiotherapy," Radiother. Oncol. **11** (4), 369-78 (1988).
[47]B. Wowk, T. Radcliffe, K. W. Leszczynski, S. Shalev and R. Rajapakshe, "Optimization of metal/phosphor screens for on-line portal imaging," Med Phys. **21** (2), 227-35 (1994).
[48]W. Swindell, E. J. Morton, P. M. Evans and D. G. Lewis, "The design of megavoltage projection imaging systems: some theoretical aspects," Med Phys. **18** (5), 855-66 (1991).

[49]J. P. Bissonnette, D. A. Jaffray, A. Fenster and P. Munro, "Optimal radiographic magnification for portal imaging," Med Phys. **21** (9), 1435-45 (1994).
[50]D. A. Jaffray, J. J. Battista, A. Fenster and P. Munro, "X-ray scatter in megavoltage transmission radiography: physical characteristics and influence on image quality," Med Phys. **21** (1), 45-60 (1994).
[51]A. L. Boyer, L. Antonuk, A. Fenster, M. Van Herk, H. Meertens, P. Munro, L. E. Reinstein and J. Wong, "A review of electronic portal imaging devices (EPIDs)," Med Phys. **19** (1), 1-16 (1992).
[52]S. Webb, *The Physics of Three Dimensional Radiation Therapy*, 1 ed. (IOP Ltd., Bristol, UK, 1993).
[53]H. Roehrig and C. Cheng, "Real-time imaging detectors for portal imaging," Proc.SPIE **2009**, 144-67 (1993).
[54]P. Munro, "Portal Imaging Technology: Past, Present and Future.," Seminars in Radiation Oncology **5**, 115-133 (1995).
[55]H. Meertens, M. van Herk and J. Weeda, "A liquid ionisation detector for digital radiography of therapeutic megavoltage photon beams," Phys. Med. Biol. **30** (4), 313-21 (1985).
[56]M. van Herk, W. Fencl and A. van Dalen, "Design and implementation of a high speed matrix ionization chamber system," Med Phys **22**, 991 (abstract) (1995).
[57]L. E. Antonuk, J. Boudry, J. Yorkston, C. F. Wild, M. J. Longo and R. A. Street, "Radiation-damage studies of amorphous-silicon photodiiode sensors for applications in radiotherapy x-ray imaging," Nucl.Inst.Meth. **A299**, 143-146 (1990).
[58]L. E. Antonuk, J. Boudry, W. Huang, D. L. McShan, E. J. Morton, J. Yorkston, M. J. Longo and R. A. Street, "Demonstration of megavoltage and diagnostic x-ray imaging with hydrogenated amorphous silicon arrays [published erratum appears in Med Phys 1993 May-Jun;20(3):825]," Med Phys. **19** (6), 1455-66 (1992).
[59]L. E. Antonuk, J. Yorkston, W. Huang, J. H. Siewerdsen, J. M. Boudry, Y. el-Mohri and M. V. Marx, "A real-time, flat-panel, amorphous silicon, digital x-ray imager," Radiographics **15** (4), 993-1000 (1995).
[60]L. E. Antonuk, J. Boudry, Y. el-Mohri, W. Huang, J. H. Siewerdsen, J. Yorkston and R. A. Street, "Large area,flat panel, amorphous silicon imagers," Proc SPIE **2432**, 216-27 (1995).
[61]L. E. Antonuk, J. Yorkston, W. Huang, H. Sandler, J. H. Siewerdsen and Y. el-Mohri, "Megavoltage imaging with a large-area, flat-panel, amorphous silicon imager," Int. J. Radiat. Oncol. Biol. Phys. **36** (3), 661-72 (1996).
[62]L. E. Antonuk, Y. el-Mohri, J. H. Siewerdsen, J. Yorkston, W. Huang, V. E. Scarpine and R. A. Street, "Empirical investigation of the signal performance of a high-resolution, indirect detection, active matrix flat-panel imager (AMFPI) for fluoroscopic and radiographic operation," Med Phys. **24** (1), 51-70 (1997).
[63]J. P. Bissonnette, I. A. Cunningham and P. Munro, "Optimal phosphor thickness for portal imaging," Med Phys. **24** (6), 803-14 (1997).
[64]D. G. Drake, D. A. Jaffray and J. W. Wong, "Prototype amorphous silicon array based radiotherapy portal imager," Proc SPIE **3032**, 32-41 (1997).
[65]J. R. Earnhart and E. L. Chaney, "Modulation transfer function for a large-area amorphous silicon image receptor," Phys. Med. Biol. **42** (12), 2531-40 (1997).
[66]M. C. Kirby and P. C. Williams, "Measurement possibilities using an electronic portal imaging device," Radiother. Oncol. **29** (2), 237-43 (1993).
[67]M. C. Kirby and P. C. Williams, "The use of an electronic portal imaging device for exit dosimetry and quality control measurements," Int. J. Radiat. Oncol. Biol. Phys. **31** (3), 593-603 (1995).
[68]H. D. Kubo, E. G. Shapiro and E. J. Seppi, "Potential and role of a prototype amorphous silicon array electronic portal imaging device in breathing synchronized radiotherapy," Med Phys. **26** (11), 2410-4 (1999).
[69]K. S. Lam, M. Partowmah and W. C. Lam, "An on-line electronic portal imaging system for external beam radiotherapy," Br. J. Rdiol. **59** (706), 1007-13 (1986).
[70]P. Munro and D. C. Bouius, "X-ray quantum limited portal imaging using amorphous silicon flat-panel arrays," Med Phys. **25** (5), 689-702 (1998).
[71]M. J. Powell, J. R. Hughes, N. C. Bird, C. Glasse and T. R. King, "Seamless tiling of amorphous silicon photodiode-TFT arrays for very large area X-ray image sensors [letter]," IEEE Transactions on Medical Imaging **17** (6), 1080-3 (1998).
[72]D. Verellen, W. De Neve, F. Van den Heuvel, M. Coghe, O. Louis and G. Storme, "On-line portal imaging: image quality defining parameters for pelvic fields--a clinical evaluation," Int. J. Radiat. Oncol. Biol. Phys. **27** (4), 945-52 (1993).
[73]J. H. Siewerdsen and D. A. Jaffray, "A ghost story: spatio-temporal response characteristics of an indirect-detection flat-panel imager," Med Phys. **26** (8), 1624-41 (1999).

[74]Y. El-Mohri, L. E. Antonuk, J. Yorkston, K. W. Jee, M. Maolinbay, K. L. Lam and J. H. Siewerdsen, "Relative dosimetry using active matrix flat-panel imager (AMFPI) technology," Med Phys. **26** (8), 1530-41 (1999).
[75]D. Mah, J. A. Rawlinson and J. A. Rowlands, "Detective quantum efficiency of an amorphous selenium detector to megavoltage radiation," Phys. Med. Biol. **44** (5), 1369-84 (1999).
[76]T. Falco, H. Wang and B. G. Fallone, "Preliminary study of a metal/a-Se-based portal detector," Med Phys. **25** (6), 814-23 (1998).
[77]M. Lachaine and B. G. Fallone, "Monte Carlo detective quantum efficiency and scatter studies of a metal/a-Se portal detector," Med Phys. **25** (7 Pt 1), 1186-94 (1998).
[78]D. Mah, J. A. Rowlands and J. A. Rawlinson, "Portal imaging with amorphous selenium: demonstration of image quality using a photoinduced discharge approach," Med Phys **23**, (abstract) (1996).
[79]D. Mah, J. A. Rowlands and J. A. Rawlinson, "Sensitivity of amorphous selenium to x rays from 40 kVp to 18 MV: measurements and implications for portal imaging," Med Phys. **25** (4), 444-56 (1998).
[80]H. Wang, T. Falco and B. G. Fallone, "A metal screen-amorphous selenium based image receptor in megavoltage portal imaging," Med Phys **23**, 1130 (abstract) (1996).
[81]W. Zhao and J. A. Rowlands, "Large-area solid state detector for radiology using amorphous selenium," Proc.SPIE **1651**, 134-143 (1992).
[82]W. Zhao and J. A. Rowlands, "Digital radiology using self-scanned readout of amorphous selenium," Proc.SPIE **1896**, 114-120 (1993).
[83]W. Zhao and J. A. Rowlands, "X-ray imaging using amorphous selenium: feasibility of a flat panel self-scanned detector for digital radiology," Med Phys **22**, 1595-1604 (1995).
[84]W. Zhao, J. Rowlands, A. S. Germann, D. Waechter and Z. J. Huang, "Digital radiology using self-scanned readout of amorphous selenium: design considerations for mammography," Proc. SPIE **2432**, 250-259 (1995).
[85]W. Zhao, I. Blevis, A. S. Germann, J. Rowlands, D. Waechter and Z. J. Huang, "Flat panel detector for digital radiology using active matrix readout of amorphous selenium," Proc. SPIE **2708**, 523-531 (1996).
[86]J. Balter, A. Thompson and R. K. Ten Haken, "Automated quality assurance of mechanical components of a computer controlled accelerator using and EPID," 4th International Workshop on Electronic Portal Imaging, Amsterdam (1996).
[87]Y. Zhu, X. Q. Jiang and J. Van Dyk, "Portal dosimetry using a liquid ion chamber matrix: dose response studies," Med Phys. **22** (7), 1101-6 (1995).
[88]R. Rajapakshe, K. Luchka and S. Shalev, "A quality control test for electronic portal imaging devices," Med Phys. **23** (7), 1237-44 (1996).
[89]D. S. Fritsch, S. Raghavan, A. Boxwala, J. Earnhart, G. Tracton, T. Cullip and E. L. Chaney, "Benchmark test cases for evaluation of computer-based methods for detection of setup errors: realistic digitally reconstructed electronic portal images with known setup errors," Int. J. Radiat. Oncol. Biol. Phys. **37** (1), 199-204 (1997).
[90]M. G. Herman, J. J. Kruse and C. Hagness, "A Guide to Clinical Implementation of Electronic Portal Imaging," J Applied Clinical Medical Physics **1**(2), 38-57 (2000).
[91]C. L. Thomason, "Implementation and clinical use of portal imaging," Cancer Treatment & Research **93**, 69-99 (1998).
[92]K. W. Leszczynski, S. Shalev and S. Ryder, "A study on the efficacy of digital enhancement of on-line portal images [published erratum appears in Med Phys 1993 Jan-Feb;20(1):255]," Med Phys. **19** (4), 999-1005 (1992).
[93]J. M. Balter, C. A. Pelizzari and G. T. Chen, "ROC evaluation of digital enhancement techniques for portal images," Med Phys **16**, 455 (abstract) (1989).
[94]W. K. Pratt, *Digital Image Processing* (Wiley, New York, 1978).
[95]C. E. Metz, H. P. Chan, K. Doi and J. H. Shen, "Contrast enhancement of noisy images by windowing: limitations due to the finite dynamic range of the display system," Med Phys. **16** (2), 170-8 (1989).
[96]R. N. Bracewell, *Two-dimensional imaging* (Prentice Hall, Englewood Cliffs, N.J, 1995).
[97]H. Meertens, M. van Herk and J. Weeda, "An inverse filter for digital restoration of portal images," Phys. Med. Biol. **33** (6), 687-702 (1988).
[98]P. H. Vos, "On-line repositioning based on portal imaging in clinical routine," 5th International Workshop on Electronic Portal Imaging , Phoenix, AZ, 45 (abstract) (1998).
[99]J. M. Balter, C. A. Pelizzari and G. T. Chen, "Correlation of projection radiographs in radiation therapy using open curve segments and points," Med Phys. **19** (2), 329-34 (1992).
[100]S. M. Jones and A. L. Boyer, "Investigation of an FFT-based correlation technique for verification of radiation treatment setup," Med Phys. **18** (6), 1116-25 (1991).

[101]J. Moseley and P. Munro, "A semiautomatic method for registration of portal images," Med Phys. **21** (4), 551-8 (1994).
[102]L. Dong and A. L. Boyer, "A portal image alignment and patient setup verification procedure using moments and correlation techniques," Phys. Med. Biol. **41** (4), 697-723 (1996).
[103]K. G. Gilhuijs, A. Touw, M. van Herk and R. E. Vijlbrief, "Optimization of automatic portal image analysis," Med Phys. **22** (7), 1089-99 (1995).
[104]D. S. Fritsch, E. L. Chaney, A. Boxwala, M. J. McAuliffe, S. Raghavan, A. Thall and J. R. Earnhart, "Core-based portal image registration for automatic radiotherapy treatment verification," Int. J. Radiat. Oncol. Biol. Phys. **33** (5), 1287-300 (1995).
[105]J. Bijhold, M. van Herk, R. Vijlbrief and J. V. Lebesque, "Fast evaluation of patient set-up during radiotherapy by aligning features in portal and simulator images," Phys. Med. Biol. **36** (12), 1665-79 (1991).
[106]K. Eilertsen, "Automatic detection of single MLC leaf positions with corrections for penumbral effects and portal imager dose rate characteristics," Phys. Med. Biol. **42** (2), 313-34 (1997).
[107]H. Wang and B. G. Fallone, "A robust morphological algorithm for automatic radiation field extraction and correlation of portal images," Med Phys. **21** (2), 237-44 (1994).
[108]H. Wang and B. G. Fallone, "A mathematical model of radiation field edge localization," Med Phys. **22** (7), 1107-10 (1995).
[109]K. G. Gilhuijs, K. Drukker, A. Touw, P. J. van de Ven and M. van Herk, "Interactive three dimensional inspection of patient setup in radiation therapy using digital portal images and computed tomography data," Int. J. Radiat. Oncol. Biol. Phys. **34** (4), 873-85 (1996).
[110]K. G. Gilhuijs, P. J. van de Ven and M. van Herk, "Automatic three-dimensional inspection of patient setup in radiation therapy using portal images, simulator images, and computed tomography data," Med Phys. **23** (3), 389-99 (1996).
[111]M. J. Murphy, "An automatic six-degree-of-freedom image registration algorithm for image-guided frameless stereotaxic radiosurgery," Med Phys. **24** (6), 857-66 (1997).
[112]A. E. Lujan, J. M. Balter and R. K. Ten Haken, "Determination of rotations in three dimensions using two-dimensional portal image registration," Med Phys. **25** (5), 703-8 (1998).
[113]W. De Neve, F. Van den Heuvel, M. Coghe, D. Verellen, M. De Beukeleer, A. Roelstraete, P. De Roover, L. Thon and G. Storme, "Interactive use of on-line portal imaging in pelvic radiation," Int. J. Radiat. Oncol. Biol. Phys. **25** (3), 517-24 (1993).
[114]P. Bergstrom, P. O. Lofroth and A. Widmark, "High-precision conformal radiotherapy (HPCRT) of prostate cancer--a new technique for exact positioning of the prostate at the time of treatment," Int. J. Radiat. Oncol. Biol. Phys. **42** (2), 305-11 (1998).
[115]J. M. Balter, G. T. Chen, C. A. Pelizzari, S. Krishnasamy, S. Rubin and S. Vijayakumar, "Online repositioning during treatment of the prostate: a study of potential limits and gains," Int. J. Radiat. Oncol. Biol. Phys. **27** (1), 137-43 (1993).
[116]K. Hatherly, J. Smylie and A. Rodger, "A comparison of field-only electronic portal imaging hard copies with double exposure port films in radiation therapy treatment setup confirmation to determine its clinical application in a radiotherapy center," Int. J. Radiat. Oncol. Biol. Phys. **45** (3), 791-6 (1999).
[117]W. C. Lam, M. Partowmah, D. J. Lee, M. D. Wharam and K. S. Lam, "On-line measurement of field placement errors in external beam radiotherapy," Br. J. Rdiol. **60** (712), 361-5 (1987).
[118]M. L. Graham, A. Y. Cheng, L. Y. Geer, W. R. Binns, M. W. Vannier and J. W. Wong, "A method to analyze 2-dimensional daily radiotherapy portal images from an on-line fiber-optic imaging system," Int. J. Radiat. Oncol. Biol. Phys. **20** (3), 613-9 (1991).
[119]J. M. Michalski, J. W. Wong, R. L. Gerber, D. Yan, A. Cheng, M. V. Graham, M. A. Renna, P. J. Sawyer and C. A. Perez, "The use of on-line image verification to estimate the variation in radiation therapy dose delivery," Int. J. Radiat. Oncol. Biol. Phys. **27** (3), 707-16 (1993).
[120]A. A. el-Gayed, A. Bel, R. Vijlbrief, H. Bartelink and J. V. Lebesque, "Time trend of patient setup deviations during pelvic irradiation using electronic portal imaging," Radiother. Oncol. **26** (2), 162-71 (1993).
[121]D. A. Fein, K. P. McGee, T. E. Schultheiss, B. L. Fowble and G. E. Hanks, "Intra- and interfractional reproducibility of tangential breast fields: a prospective on-line portal imaging study," Int. J. Radiat. Oncol. Biol. Phys. **34** (3), 733-40 (1996).

[122]M. G. Herman, K. O. Khadivi, I. Gage, L. Kleinberg and R. A. Abrams, "Effects of respiration on target and critical structure positions during treatment assessed with movie-loop electronic portal imaging," Int. J. Radiat. Oncol. Biol. Phys. **39 2S** ((abstract)), 163 (1997).
[123]E. Vigneault, J. Pouliot, J. Laverdiere, J. Roy and M. Dorion, "Electronic portal imaging device detection of radioopaque markers for the evaluation of prostate position during megavoltage irradiation: a clinical study," Int. J. Radiat. Oncol. Biol. Phys. **37** (1), 205-12 (1997).
[124]A. Tinger, J. M. Michalski, W. R. Bosch, R. K. Valicenti, D. A. Low and R. J. Myerson, "An analysis of intratreatment and intertreatment displacements in pelvic radiotherapy using electronic portal imaging," Int. J. Radiat. Oncol. Biol. Phys. **34** (3), 683-90 (1996).
[125]D. Yan, J. W. Wong, G. Gustafson and A. Martinez, "A new model for "accept or reject" strategies in off-line and on-line megavoltage treatment evaluation," Int. J. Radiat. Oncol. Biol. Phys. **31** (4), 943-52 (1995).
[126]D. Yan, J. Wong, F. Vicini, J. Michalski, C. Pan, A. Frazier, E. Horwitz and A. Martinez, "Adaptive modification of treatment planning to minimize the deleterious effects of treatment setup errors," Int. J. Radiat. Oncol. Biol. Phys. **38** (1), 197-206 (1997).
[127]J. W. Denham, M. J. Dally, K. Hunter, J. Wheat, P. P. Fahey and C. S. Hamilton, "Objective decision-making following a portal film: the results of a pilot study," Int. J. Radiat. Oncol. Biol. Phys. **26** (5), 869-76 (1993).
[128]C. D. Mubata, A. M. Bidmead, L. M. Ellingham, V. Thompson and D. P. Dearnaley, "Portal imaging protocol for radical dose-escalated radiotherapy treatment of prostate cancer," Int. J. Radiat. Oncol. Biol. Phys. **40** (1), 221-31 (1998).
[129]S. Lavertu, L. M. Girouard and J. Pouliot, "Observation study of electronic portal images for off-line verification," Radiother. Oncol. **54** (1), 47-55 (2000).
[130]D. Yan, D. Lockman, D. Brabbins, L. Tyburski and A. Martinez, "An off-line strategy for constructing a patient-specific planning target volume in adaptive treatment process for prostate cancer," Int. J. Radiat. Oncol. Biol. Phys. **48** (1), 289-302 (2000).
[131]K. Luchka, D. Chen, S. Shalev, G. Gluhchev and R. Rajapakshe, "Assessing radiation and light field congruence with a video based electronic portal imaging device," Med Phys. **23** (7), 1245-52 (1996).
[132]P. Dunscombe, S. Humphreys and K. Leszczynski, "A test tool for the visual verification of light and radiation fields using film or an electronic portal imaging device," Med Phys. **26** (2), 239-43 (1999).
[133]L. Dong, A. Shiu, S. Tung and A. Boyer, "Verification of radiosurgery target point alignment with an electronic portal imaging device (EPID)," Med Phys. **24** (2), 263-7 (1997).
[134]P. McGhee, T. Chu, K. Leszczynski and P. Dunscombe, "The Siemens virtual wedge," Medical Dosimetry **22** (1), 39-41 (1997).
[135]J. M. Balter, D. L. McShan, J. J. Kim and B. A. Fraass, "Automated verification of dynamic multileaf configuration using a megavoltage imager and a computer controlled radiotherapy system," Med Phys **24** (6), 1002(abstract) (1997).
[136]M. Partridge, P. M. Evans, A. Mosleh-Shirazi and D. Convery, "Independent verification using portal imaging of intensity-modulated beam delivery by the dynamic MLC technique," Med Phys. **25** (10), 1872-9 (1998).
[137]F. F. Yin, M. C. Schell and P. Rubin, "A technique of automating compensator design for lung inhomogeneity correction using an electron portal imaging device," Med Phys. **21** (11), 1729-32 (1994).
[138]P. M. Evans, V. N. Hansen, W. P. Mayles, W. Swindell, M. Torr and J. R. Yarnold, "Design of compensators for breast radiotherapy using electronic portal imaging," Radiother. Oncol. **37** (1), 43-54 (1995).
[139]P. M. Evans, E. M. Donovan, N. Fenton, V. N. Hansen, I. Moore, M. Partridge, S. Reise, B. Suter, J. R. Symonds-Tayler and J. R. Yarnold, "Practical implementation of compensators in breast radiotherapy," Radiother. Oncol. **49** (3), 255-65 (1998).
[140]H. Parsaei, S. Hussein and E. el-Khatib, "Lung compensator design using an electronic portal imaging device," Medical Dosimetry **24** (1), 67-71 (1999).
[141]D. A. Low, Z. Li and E. E. Klein, "Verification of milled two-dimensional photon compensating filters using an electronic portal imaging device," Med Phys. **23** (6), 929-38 (1996).
[142]K. L. Pasma, M. Kroonwijk, E. B. van Dieren, A. G. Visser and B. J. Heijmen, "Verification of compensator thicknesses using a fluoroscopic electronic portal imaging device," Med Phys. **26** (8), 1524-1529 (1999).
[143]E. M. Donovan, U. Johnson, G. Shentall, P. M. Evans, A. J. Neal and J. R. Yarnold, "Evaluation of compensation in breast radiotherapy: a planning study using multiple static fields," Int. J. Radiat. Oncol. Biol. Phys. **46** (3), 671-9 (2000).

[144]H. V. James, S. Atherton, G. J. Budgell, M. C. Kirby and P. C. Williams, "Verification of dynamic multileaf collimation using an electronic portal imaging device," Phys. Med. Biol. **45** (2), 495-509 (2000).
[145]J. Chang, G. S. Mageras, C. S. Chui, C. C. Ling and W. Lutz, "Relative profile and dose verification of intensity-modulated radiation therapy," Int. J. Radiat. Oncol. Biol. Phys. **47** (1), 231-40 (2000).
[146]A. J. Curtin-Savard and E. B. Podgorsak, "Verification of segmented beam delivery using a commercial electronic portal imaging device," Med Phys. **26** (5), 737-42 (1999).
[147]B. J. Heijmen, K. L. Pasma, M. Kroonwijk, V. G. Althof, J. C. de Boer, A. G. Visser and H. Huizenga, "Portal dose measurement in radiotherapy using an electronic portal imaging device (EPID)," Phys. Med. Biol. **40** (11), 1943-55 (1995).
[148]M. Essers, R. Boellaard, M. van Herk, H. Lanson and B. Mijnheer, "Transmission dosimetry with a liquid-filled electronic portal imaging device," Int. J. Radiat. Oncol. Biol. Phys. **34** (4), 931-41 (1996).
[149]V. N. Hansen, P. M. Evans and W. Swindell, "The application of transit dosimetry to precision radiotherapy," Med Phys. **23** (5), 713-21 (1996).
[150]T. R. McNutt, T. R. Mackie, P. Reckwerdt, N. Papanikolaou and B. R. Paliwal, "Calculation of portal dose using the convolution/superposition method," Med Phys. **23** (4), 527-35 (1996).
[151]R. Boellaard, M. van Herk and B. J. Mijnheer, "A convolution model to convert transmission dose images to exit dose distributions," Med Phys. **24** (2), 189-99 (1997).
[152]R. Boellaard, M. van Herk, H. Uiterwaal and B. Mijnheer, "First clinical tests using a liquid-filled electronic portal imaging device and a convolution model for the verification of the midplane dose," Radiother. Oncol. **47** (3), 303-12 (1998).
[153]R. Boellaard, M. Essers, M. van Herk and B. J. Mijnheer, "New method to obtain the midplane dose using portal in vivo dosimetry," Int. J. Radiat. Oncol. Biol. Phys. **41** (2), 465-74 (1998).
[154]H. Keller, M. Fix and P. Ruegsegger, "Calibration of a portal imaging device for high-precision dosimetry: a Monte Carlo study," Med Phys. **25** (10), 1891-902 (1998).
[155]M. Kroonwijk, K. L. Pasma, S. Quint, P. C. Koper, A. G. Visser and B. J. Heijmen, "In vivo dosimetry for prostate cancer patients using an electronic portal imaging device (EPID); demonstration of internal organ motion," Radiother. Oncol. **49** (2), 125-32 (1998).
[156]H. Parsaei, E. el-Khatib and R. Rajapakshe, "The use of an electronic portal imaging system to measure portal dose and portal dose profiles [published erratum appears in Med Phys 1999 Feb;26(2):331]," Med Phys. **25** (10), 1903-9 (1998).
[157]K. L. Pasma, M. Kroonwijk, J. C. de Boer, A. G. Visser and B. J. Heijmen, "Accurate portal dose measurement with a fluoroscopic electronic portal imaging device (EPID) for open and wedged beams and dynamic multileaf collimation," Phys. Med. Biol. **43** (8), 2047-60 (1998).
[158]X. He, A. Van Esch, R. Reymen and D. Huyskens, "Evaluation of an electronic portal imaging device for transit dosimetry," Acta Oncologica **38** (5), 591-6 (1999).
[159]K. L. Pasma, M. Kroonwijk, S. Quint, A. G. Visser and B. J. Heijmen, "Transit dosimetry with an electronic portal imaging device (EPID) for 115 prostate cancer patients," Int. J. Radiat. Oncol. Biol. Phys. **45** (5), 1297-303 (1999).
[160]J. C. de Boer, B. J. Heijmen, K. L. Pasma and A. G. Visser, "Characterization of a high-elbow, fluoroscopic electronic portal imaging device for portal dosimetry," Phys. Med. Biol. **45** (1), 197-216 (2000).
[161]A. G. Glendinning and D. E. Bonnett, "Dosimetric properties of the Theraview fluoroscopic electronic portal imaging device," Br. J. Rdiol. **73** (869), 517-30 (2000).
[162]K. Kesteloot, A. Dutreix and E. van der Schueren, "A model for calculating the costs of in vivo dosimetry and portal imaging in radiotherapy departments," Radiother. Oncol. **28** (2), 108-17 (1993).

TABLES II-VI

Table II. Features of the Five Commercially Available EPIDs.

Supplier	Elekta	Eliav	Cablon	Siemens	Varian
Name	SRI 100	PortPro	Theraview	Beamview Plus	PortalVision
Type	CCD Camera	CCD camera	Plumbicon camera	Newvicon camera	Matrix ion chamber
Detector pixels	512 x 512	512 x 512	512 x 512	512 x 512	256 x 256
Digitization	8-bit frame-grabber	8-bit frame-grabber	8-bit frame-grabber	8-bit frame-grabber	14-bit A/D converter
Max frequency of acquisition	7 frames/sec	30 frames/sec	2 monitor units	30 frames/sec	Mark 1: 5.5 seconds Mark 2: 1.25 seconds
x-ray Detector	1.5 mm steel plate + 411 mg/cm^2 Gd_2O_2S screen	1.5 mm steel plate + 411 mg/cm^2 Gd_2O_2S screen	1.5 mm brass plate + 400 mg/cm^2 Gd_2O_2S screen	1.2 mm brass plate + 160 mg/cm^2 Gd_2O_2S screen	1.0mm plastoferrite plate + 0.8 mm 2.24-trimethyl- pentane + wire electrodes
Mechanical assembly	Dismountable	Portable	Partly retractable and partly dismountable	Fully retractable	Fully retractable; portable if used with retractable arm
Mounting	Philips only	Any accelerator	Any accelerator (GE, Varian, Scanditronix)	Siemens only	Any accelerator (attached by customer)
Collision interlock	Yes	No	Yes (connect to accelerator motion interlocks)	No (interlock activated during deployment only)	Yes
Field of view at isocenter (cm x cm)	Fixed 19 x 24	Variable	Adjustable 31.8 dia. Varian 31.5 dia. Sanditronix 31.6 dia. G.E.	Fixed 24 x 30	Adjustable 25 x 25
Detector area (cm x cm)	30 x 38	Variable	40 x 40 (detector)	35 x 44 (detector)	32.5 x 32.5 (detector)
Detector to isocenter (cm)	60	not applicable	30-60 (Varian) 26-67 (G.E.) 27-78 (Scanditronix)	39	5-80
Display center accuracy	± 1 mm		± 5 mm	± 2 mm	± 5 mm
Prototype descriptions	Ref 49		Ref 51	Ref 53	Ref 46,47
Resolution lp/mm (Sec 4)	0.180	0.305	0.223	0.204	0.258

Table III. Summary of initial commissioning items, tolerances and methods

Item	**Purpose**	**Tolerance**	**Method/Tools**
Mechanical Stability	Safety	No accidental crash	Inspection
	Image Quality	Optical/physical Alignment (2mm)	Optical Test Pattern Optical Distance Indicators
Electrical Connections	Safety	No exposed connections/wires	Inspection of cabling/grounds
Calibration	Image quality	Acceptable flat field, dark current/noise characteristics	Per vendor follow calibration steps for energy, field size and noise. Vendor specifications vary.
Dose control	Image quality/Safety	Preset dose (linac) control functions	Program and verify correct beam termination with dose.
Image Quality	Image Quality	Acceptable contrast (1%) and spatial resolution (2-3mm)	Las Vegas Phantom, other contrast phantoms, imaged at each energy
Analysis Software	Quantitative reporting	Reported measurements within tolerance of 3mm and 2 degrees. Edge detection matches field boundary	Set up known error conditions and verify system reporting and field edge definition under varying field acquisition conditions

Table IV. Frequency of QA tasks

Interval	**Task** (P-physicist, M-manufacturer, E-engineer, T-therapist)
Daily	Inspect imager housing (T) Test collision interlock (T) Acquire day's 1st image during machine warm-up procedure to verify operation and image quality (T) Verify sufficient data capacity for day's images (P or designate)
Monthly	Acquire image and inspect for artifacts (P) Perform constancy check of SNR, resolution and localization(P) Review image quality Perform image and disk maintenance (P) Mechanical inspection (latches, collision sensors, optical components (P,E) Electrical connections (P,E) Test collision interlock (P) Hardcopy output (P)
Annual	Perform full check of geometric localization accuracy (P)

Table V. Questions that are pertinent to implement an EPID for clinical use.

Questions	Options
1. What is the purpose/goal of installing EPIDs in the clinic?	a) simple film replacement/routine QA b) accurate and efficient patient setup and re-positioning c) assess random and systematic errors in treatment d) assessment of the efficacy of immobilization techniques e) inter and intra- fraction motion studies
2. Which patients will EPID be used for treatment verification?	a) All patients? b) Special cases that are difficult to setup? c) Specific disease sites?
3. How will the EPID be used?	a) Exclusively to eliminate film b) Combine with a pre-defined port film protocol
4. What is the frequency of imaging?	a) Weekly b) Daily c) Dependent on site or patient d) Dependent on the statistics of setup error or decision rules
4a. What image acquisition modes are available on the EPID?	a) Single exposure b) Double exposure c) Movie-loops
5. What is the choice of reference image?	a) Digitally Reconstructed Radiograph b) Conventional Simulation film c) First approved EPID image
6. How will image evaluation be accomplished?	a) Electronically, side by side on computer workstation b) Hard copy on conventional view box
6a. How many review stations are needed and at what locations?	a) At each treatment machine b) Also in viewing rooms c) Also in Physicians offices
7. When will you intervene/adjust setup?	a) threshold for corrective action b) on-line - intra-fraction correction c) off-line - inter-fraction correction
8. What image analysis protocol will be used?	a) visual inspection only b) manual tools c) semi-automated d) automated
8a. Which analysis tools are available and validated on the system ?	a) visual inspection only b) manual tools c) semi-automated d) automated
9. How will physician approval be achieved?	a) Signed hard copy off-line b) Electronic signature on-line c) Electronic signature off-line
9a. How will physician comments be communicated to others?	a) Hard copy b) Electronic Annotation within EPID/information system c) Electronic email outside of EPID/information system
10. What are the resources needed for storage, archival and retrieval?	a) Standalone hard disk b) Distributed database
10a. Is the system DICOM-RT compliant?	
11. Implementation of a QA program	a) Establish baseline mechanical limits and imaging quality b) Establish daily and monthly protocol
11a. What are vendor established QA routines?	
12. How will training and education for ALL users be scheduled?	a) Establish training schedule b) Define personnel responsibilities c) Periodic in-service to ensure uniformity of clinical practice

Table VI.Approximate personnel time commitments for various tasks related to the clinical use of an EPID.

Task		**Time**	**per**	**Personnel**	**Comment**
Acceptance Testing		1-2 days	Installation		additional
Education	Expert	2 days+	Installation	Physicist	per software
	Therapist	1 day	Installation	Therapist	
	Physician	½ day	Installation	Physician	revision
Establish QA Program		½ day	Installation	Physicist	Plus ongoing monitoring
Operation	Imaging	<1-2 min.	Tx. Field	Therapist	
	Review	0-5 min.	Tx. Field	Physician/ Therapist	Depends critically on mode of use – Table V
QA	Daily/ Weekly	3-5 min.	Week	Therapist	
	Monthly	30 min.	Month	Physicist	
	Quarterly	1-2 hr.	Quarter	Service	
Commissioning Correction Thresholds		1 month	Protocol	All	Software, intra and inter-user, etc.

Table VII. Current aSi Commercial Systems Available or in Beta Test.

Manufacturer	Available*	Field of view	Pixel array (cm2)	Frame rate	Acquisition	Mount
Elekta	Beta	41x41	1024x1024	3.5/s	variable	fixed
Siemens	Beta	41x41	1024x1024	3.5/s	variable	variable
Varian	Production	40x30	512x384	3/s	14bit variable	variable

* as of 6/2001